2011

EVALUATION OF MECHANICAL PROERTIES AND EFFECTIVE THICKNESS OF THE INTERFACES BY FINITE ELEMENT ANALYSIS

Sesha Spandana Pulla
University of Kentucky, spandan17@gmail.com

STUDENT AGREEMENT:

I represent that my thesis or dissertation and abstract are my original work. Proper attribution has been given to all outside sources. I understand that I am solely responsible for obtaining any needed copyright permissions. I have obtained and attached hereto needed written permission statements(s) from the owner(s) of each third-party copyrighted matter to be included in my work, allowing electronic distribution (if such use is not permitted by the fair use doctrine).

I hereby grant to The University of Kentucky and its agents the non-exclusive license to archive and make accessible my work in whole or in part in all forms of media, now or hereafter known. I agree that the document mentioned above may be made available immediately for worldwide access unless a preapproved embargo applies.

I retain all other ownership rights to the copyright of my work. I also retain the right to use in future works (such as articles or books) all or part of my work. I understand that I am free to register the copyright to my work.

REVIEW, APPROVAL AND ACCEPTANCE

The document mentioned above has been reviewed and accepted by the student's advisor, on behalf of the advisory committee, and by the Director of Graduate Studies (DGS), on behalf of the program; we verify that this is the final, approved version of the student's dissertation including all changes required by the advisory committee. The undersigned agree to abide by the statements above.

Sesha Spandana Pulla, Student

Dr. Yuebin Charles Lu, Major Professor

Dr. James McDonough, Director of Graduate Studies

EVALUATION OF MECHANICAL PROERTIES AND EFFECTIVE THICKNESS OF THE INTERFACES BY FINITE ELEMENT ANALYSIS

THESIS

A thesis submitted in partial fulfillment of the
requirements for the degree of Master of Science in Mechanical Engineering
in the College of Engineering
at the University of Kentucky

By

SESHA SPANDANA PULLA

Lexington, Kentucky

Director: Dr. Yuebin Charles Lu, Assistant Professor of Mechanical Engineering
Lexington, Kentucky

2011

ABSTRACT OF THE THESIS

EVALUATION OF MECHANICAL PROPERTIES AND EFFECTIVE THICKNESS OF THE INTERFACES BY FINITE ELEMENT ANALYSIS

The nanoindentation technique has been used to identify the interfaces between dissimilar materials and subsequently to evaluate the physical and mechanical properties across the interfaces. The interfaces could represent the interface (transition face) between oxidized and unoxidized polymers, the interface between rigid fiber and polymer matrix, or other similar situations. It is proposed to use a nanoindenter equipped with small spherical tip to indent across the interfaces of dissimilar materials. The proposed method has been validated by conducting a large number of virtual experiments through 3-dimensional finite element simulations, by varying the properties of the two dissimilar materials, including various combinations of modulus (E_1/E_2), yield strength (σ_{y1}/σ_{y2}), hardening index (n_1/n_2), interface sizes (R/T), Poisson's ratio (ν), etc. The mechanical properties across the interfaces have been obtained, and a quantitative model for predicting the interface sizes has been established.

KEYWORDS: Nanoindentation; Interfacial thickness; Polymer interfaces; Finite element method.

Sesha Spandana Pulla

DATE: 07/13/2011

EVALUATION OF MECHANICAL PROERTIES AND EFFECTIVE THICKNESS OF THE INTERFACES BY FINITE ELEMENT ANALYSIS

By

Sesha Spandana Pulla

Dr. Yuebin Charles Lu

Director of Thesis

Dr. James McDonough

Director of Graduate Studies

Date: 08/16/2011

Dedicated to my father Pulla Sankara Rao, who constantly encouraged and motivated me throughout my career to achieve my goals, my mother Chillarige Uma, who inspired me to have patience and perseverance to fulfill my dreams and my brother Pulla Sudheendra Rajan, for his care and affection that truly added joy to the whole journey.

ACKNOWLEDGEMENTS

I would like to express my immense respect and gratitude to my academic advisor Dr.Y. Charles Lu who not only believed in me but also supported and guided me throughout my graduate academic career by giving me his valuable advice and great opportunity to advance my research interests.

I would like to thank the NASA EPSCoR Research Infrastructure Development (RID) Program for their financial support that made this project possible.

I would like to express my deepest gratitude to my best friend Madhu Shree Akasapu, who encouraged me to pursue my higher studies and guided me from the beginning. I would also like to thank my dear ones Brian Hampton, and friends Vivek Hariharan, Jared Fulcher, Ning Zhang and my relatives who motivated me throughout the process.

Lastly, I would like to express my appreciation and gratitude to Dr. Tingwen Wu and Dr. Haluk Karaca for accepting my request to be a part of my thesis committee and for taking time for my defense apart from of their busy schedules.

TABLE OF CONTENTS

LIST OF TABLES

LIST OF FIGURES

CHAPTER 1 - INTRODUCTION

1.1 Background

Polymer matrix composites (PMCs) have been increasingly used for high temperature applications in automotive and aerospace industries. Example applications include the automotive engine covers and turbine engine exhaust structures. The matrix systems in the high temperature PMCs are predominantly thermoset polymers. These polymers are chosen since they have highly cross-linked structures that form during the curing process. Typical thermosets include polyimides, epoxies, unsaturated polyesters, vinyl esters, etc. One of the major concerns in using polymer matrix composites at high temperature environments is the thermo-oxidative degradation of the polymer matrix and the matrix-fiber interfaces. Exposed to elevated temperature, the free surfaces of PMCs are susceptible to oxidation. When exposed to thermo-mechanical loading, the result is accelerated degradation and ply cracking which in turn introduces new free surfaces. Ultimately, the thermo-oxidative degradation reduces the life and durability of the composite system. Thus, the ability to fully understand and characterize the physical and mechanical responses resulting from thermo-oxidative processes is paramount to the continued development and increased use of high temperature PMCs in the industry.

The degradation of polymer resins used in high temperature applications can be a result of either physical aging or chemical aging, or both. The physical aging is a thermodynamically reversible volumetric response due to slow evolution toward thermodynamic equilibrium. The decreased molecular mobility and free-volume reduction lead to strain and damage development in the material. The chemical aging is a nonreversible volumetric response due to chain-scission reactions and/or additional cross-linking, hydrolysis, depolymerization, and plasticization. A dominant chemical aging process for high temperature PMCs is thermo-oxidative aging. According to Schoeppner, et al. [1, 2], the thermo-oxidative aging of polymers is “a nonreversible, surface diffusion

response in which chemical changes occur during the oxidation of a polymer, [where] oxidation leads to a reduction in molecular weight as a result of chemical bond breakage and weight loss due to out-gassing of low-molecular weight gaseous species."

A three-region model has been proposed by Tandon, et al [3], to explain the mechanism of the thermo-oxidative degradation in polymers. According to this model, the surface oxidative layer is separated from the unoxidized polymer with an active reaction zone (Figure 1.1). The oxygen (O_2) in air diffuses through the polymer and then consumed by the oxidation reaction. The parameter ϕ shown in Figure 1.1 is called the polymer availability state variable and the parameter ϕ_{ox} characterizes the completely oxidized polymer. Once a region is fully oxidized (called the Oxidized Layer), the oxidation reaction is terminated and oxygen can diffuse through it. Then, oxygen begins to react in the adjoining region (called the Transition Region), where $\phi_{ox}<\phi<1$. In the region far from the exposed surface (called the Unoxidized Interior), no polymer has been oxidized ($\phi=1$).

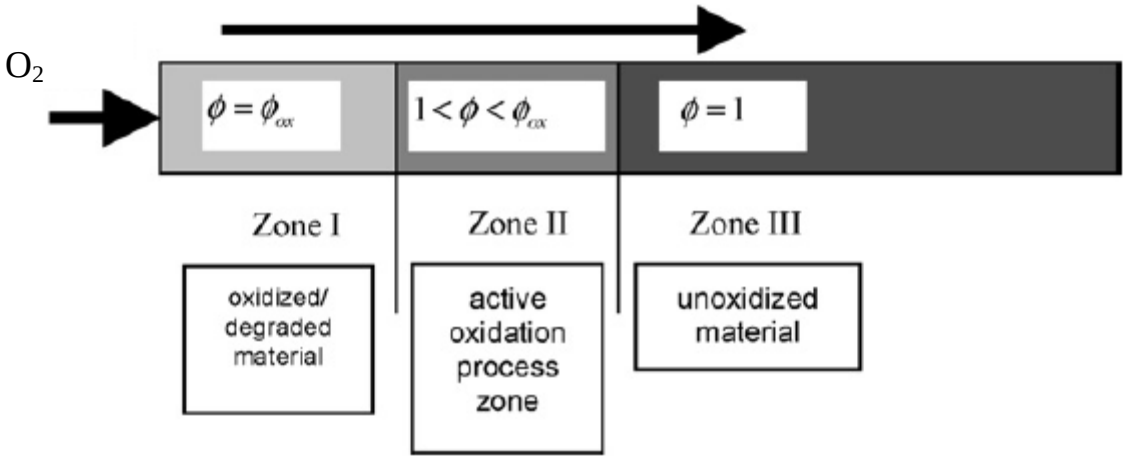

Figure 1.1 Schematic of the three-zones in thermo-oxidation of polymers [3].

Because of the thermo-oxidative degradation, it is expected that the physical and mechanical properties will change in the polymer resins. However, depending upon the material systems, it can be rather difficult to observe and characterize such changes by using conventional techniques, such as the light microscopy, scanning electron

microscopy, etc. Figure 1.2(a) shows a photomicrograph of PMR-15 polymer resin isothermally aged in ambient air at 343°C for a period of 196 hrs [4]. The optical micrograph clearly shows the three regions due to oxidation: oxidized region, transition region, and unoxidized region. This observation at least helps measuring and characterization of the transition region, although the exact boundaries of the transition zone are still hard to be determined. Figure 1.2(b) is the photomicrograph of the AFR-PE-4 polymer resin aged for 1200 hrs at 343°C [4]. Unlike PMR-15, the oxidized layer could not be observed for AFR-PE-4 by light microscopy. Thus, new technique for identifying and characterizing the interface (transition zone) is needed.

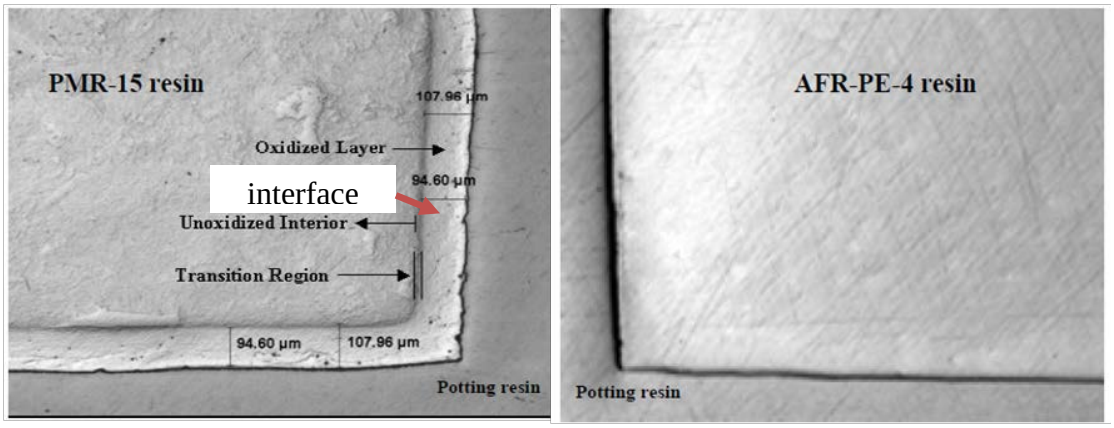

Figure 1.2 Photomicrographs showing the structure changes due to thermo-oxidization. (a) PMR-15 resin after 196 hrs of aging at 343°C; (b) AFR-PE-4 resin after 1200 hrs of aging at 343°C [4].

Similar issue can be extended to the interfaces in the fiber reinforced polymer composites [5]. The interface between reinforcing fibers and matrix is believed to play an important role in the overall composite properties (Figure 1.3). However, due to the small size, it is often difficult to properly characterize the properties of the interfaces.

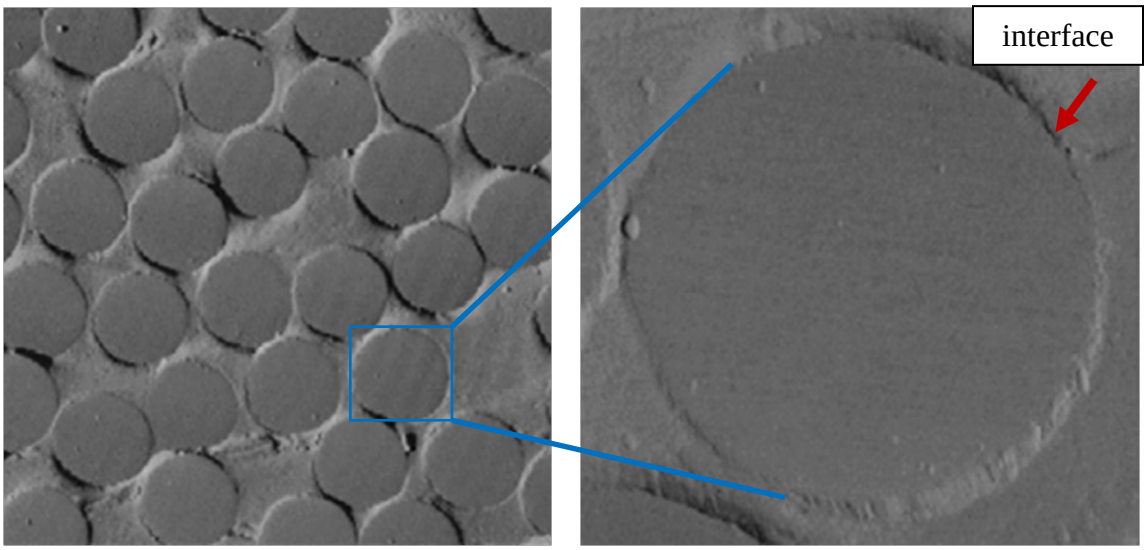

Figure 1.3 Photomicrographs showing the interface at the fiber reinforced polymer composites [5].

1.2 Objectives of the Thesis

This thesis proposes the use of nanoindentation method to identify the interface between dissimilar materials and subsequently to evaluate the physical and mechanical properties across the interface. It is proposed to use a nanoindenter with spherical tip to indent the interface between dissimilar material, which could represent the interface (transition face) between oxidized and unoxidized polymers, the interface between rigid fiber and polymer matrix, or other similar situations. The nanoindentation test will be simulated by using the finite element method. To evaluate the effective size (thickness) and the properties of the interface, a series of nanoindentation tests are conducted with the spherical indenter across the interface. Various interface scenarios will be considered by varying the properties of the two dissimilar materials, including various combinations of modulus, yield strength, hardening index, and interface sizes. Methods will be developed to predict the sizes (thickness) of the interfaces as well as their mechanical properties.

1.3 Organization of the Thesis

Chapter 2 gives the review of literatures on the characterization of interface of dissimilar materials (primarily the thermo-oxidized polymers) and the use of nanoindentation

technique. Chapter 3 presents the detailed procedures of the finite element modeling of interfaces. Results and discussion are given in Chapter 4, including the mechanical properties at the interfaces and the estimation of effective thickness of the interfaces. Finally Chapter 5 includes the summary of the present work and the scope of possible future work related to the interface research.

CHAPTER 2 - REVIEW OF LITERATURES

2.1 Characterization of Interface of Dissimilar Materials

The interface is defined as a region that separates two dissimilar materials. In the present study, our primary interest is the interface between oxidized and unoxidized polymer resins, which exists in polymer matrix composites used at elevated temperatures.

Hot structures for helicopters and aircrafts are subjected to severe thermo-mechanical conditions for the long periods of time. This kind of exposure to drastic conditions at high temperatures has significant effects on the performance of these structures. When these materials are exposed to high temperatures and to oxygen, thermo-oxidative degradation of the polymer resin occurs. The oxidative degradation occurs at the exposed surfaces causing the oxygen to diffuse into the polymer resin. This causes the formation of the oxidized layer due to the chemical reaction taking place between the exposed surface of the polymer resin and oxygen. Thus oxidized region, interface and the unoxidized region are the three regions formed in the polymer resin due to the thermo-oxidative degradation, as shown in (Figure 2.1).

The identifications of the oxidized regions in high temperature polymer resins have been mostly achieved through various optical techniques, such as dark-field imaging, polarized light microscopy, and scanning electron microscopy in backscatter mode. With optical microscope (Nikon Microphoto-FXL, Model F84006) using a bright-field light, Lu et al [6] had examined the oxidized PMR-15 resin (Figure 2.1).Polymerization of monomeric reactants (PMR-15), originally developed by NASA Lewis Research Center in 1970’s, has been the most widely used resin material in high-temperature polymer matrix composites due to its thermo-oxidative stability and high glass transition temperature, Tg ~340°C, which permits composites having an extended service temperature of 288°C. The micrograph of a PMR-15 aged at 316°C for 651 h reveals the three material regions,

representing different levels of oxidation. They are: Zone I - the fully oxidized surface layer, Zone II - the interface or the transition zone (where a mix of oxidized and unoxidized polymers exist), and Zone III - an unoxidized interior. In contrast with the oxidized region, the actual size (thickness) of the interface (Zone II) is rather hard to determine. The thickness of the interface further depends upon the environmental conditions (time, temperature and pressure).

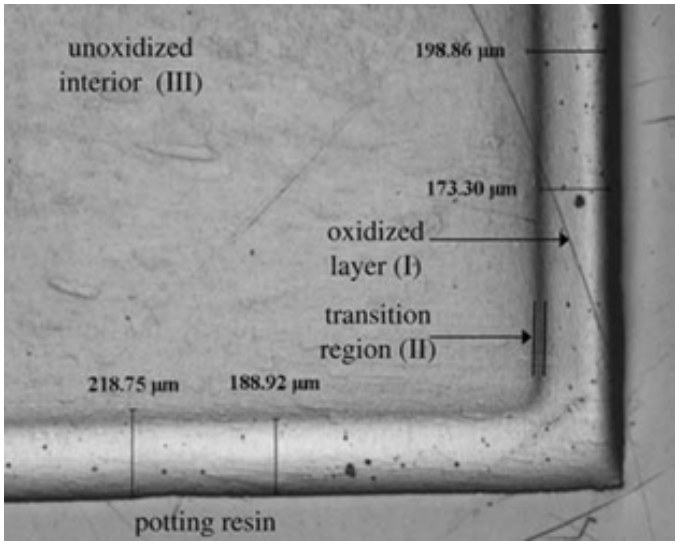

Figure 2.1 Optical micrographs of oxidized PMR-15 polymide aged at 316^{o}C for 651 h in 0.414-MPa pressurized air.

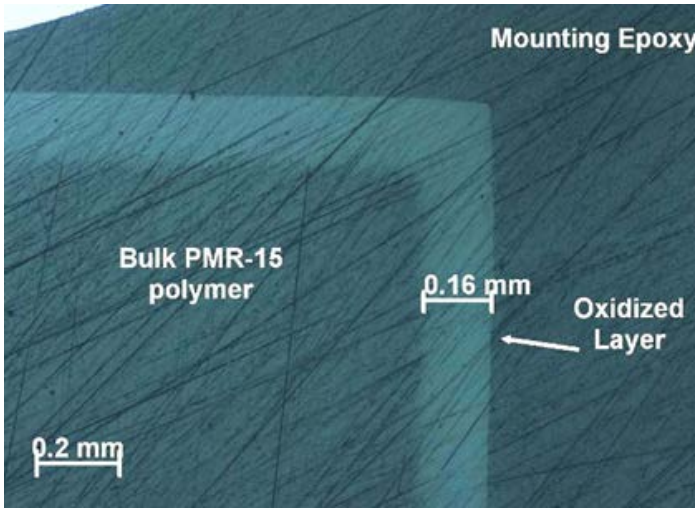

Figure 2.2 Optical micrograph showing the oxidized PMR-15 neat resin sample aged for 1000 h at 288°C in air [7].

Using a digital microscope (Nikon EPIPHOT) with fluorescence imaging technique, Broeckert [7] also obtained the picture of oxidized PMR-15 resin (Figure 2.2). Under this method, the oxidized layer is clearly different from the unoxidized region, but the interface is hard to define.

The newest ultra-high temperature polyimide resin, AFR-PE-4, is capable of withstanding long term exposure to temperatures up to 700°F (371°C). The thermo-oxidative degradation of AFR-PE-4 has been studied by Ripberger et al [4]. Figure 2.3 shows the optical microscopy image of the AFR-PE-4 specimen aged for 1200 hrs at 343^{o}C. Unlike other high temperature resins, the oxidation layers for AFR-PE-4 do not change the optical characteristics of the material, and the oxidized layer could not be observed.

Clearly, the conventional optical technique has limitations in identifying and characterizing the interfaces.

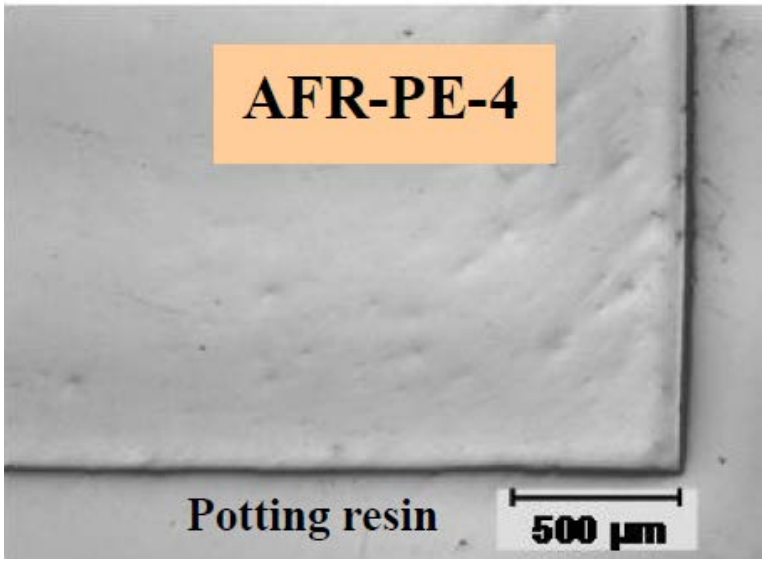

Figure 2.3 Optical micrographs showing the oxidized AFR-PE-4 neat resin aged at elevated temperature [4].

Interface study has also been a very important subject in fiber-reinforced polymer composites. The classical definition of interface in fiber reinforced composites is that "an interface is a surface formed by the common boundary of reinforcing fiber and matrix in contact which constitutes the bond in-between for transfer of load. It has physical and mechanical properties which are unique and not those of either the fiber or the matrix" [31].

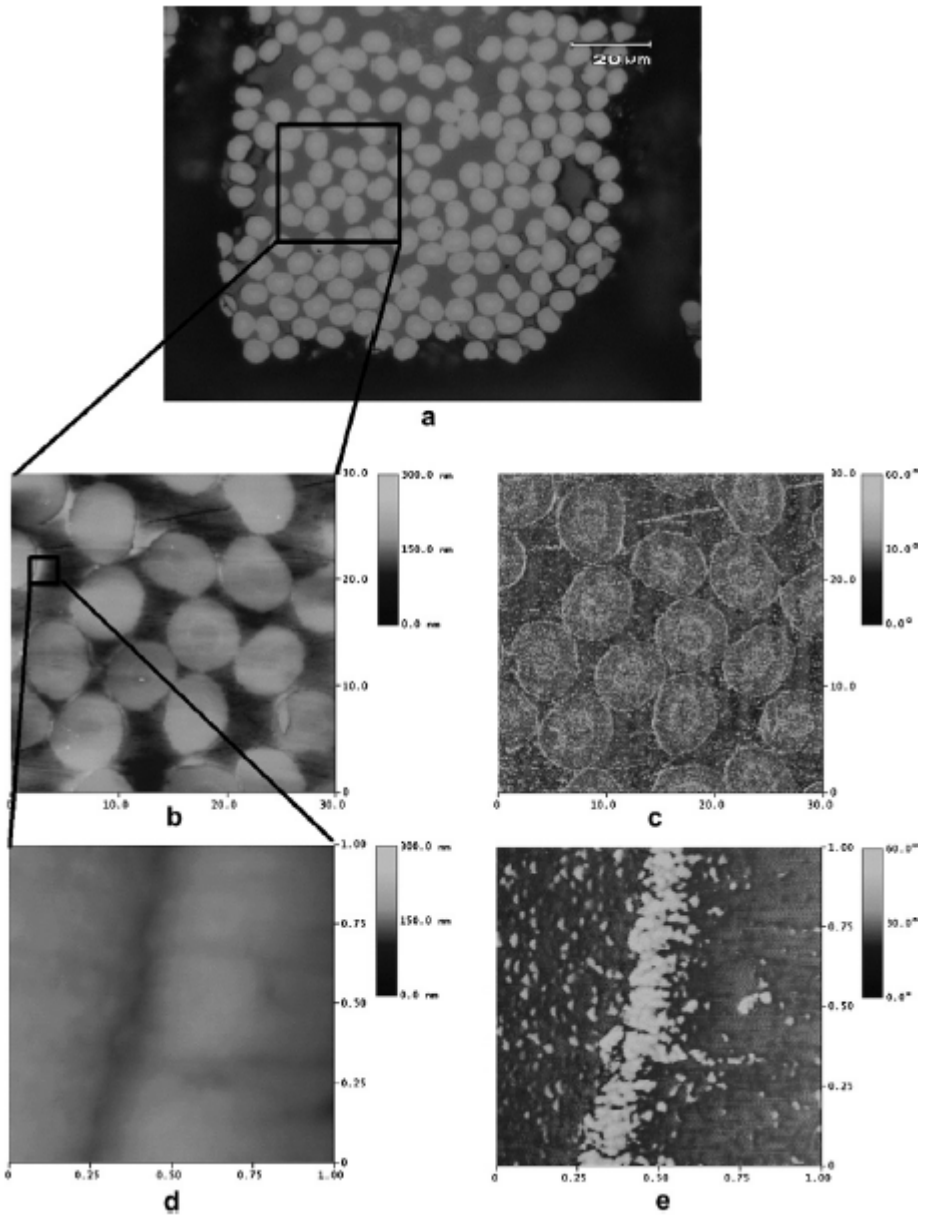

Figure 2.4 Optical micrographs showing the interface in fiber reinforced composites (a) optical micrograph of the composites, (b) height image of the cross-section, (c) phase image of cross-section, (d) height image and (e) phase image of the interface [5].

The quality of stress transfer in the interphase is the deciding factor for the performance of a composite as a structural material. The interphase in the fiber-reinforced composite material extends from a few nanometers to microns. Also, the mechanical properties in this interphase region vary continuously from those of the fiber to the polymer. And it is believed that the nature of the interphase would vary with the specific composite system [8, 9]. A properly designed interphase can help improve the performance of the structure by improving its strength, toughness and environmental stability of the composites [8]. For instance, when the interphase is made softer than the surrounding polymer it would give lower overall stiffness and strength to the composite but has greater resistance to fracture. Whereas, when an interphase is made stiffer than its surrounding polymer it leads to less fracture resistance but makes the polymer stronger and stiff. Hence, it's clear that better understanding of the interphase can help in better evaluation of the fiber-reinforced composite [8].

However, when the interphase is no more than a few microns it is difficult to be studied by conventional experimental procedures. The common methods of characterizing the interface properties in fiber reinforced composites have been testing the macroscopic size specimens: either a laminate (many fibers) or an individual fiber embedded in specially constructed matrix [32]. The specimens are tested in the mode of either tension, compression, or shear, from which the properties of the interface are extrapolated [32]. The results obtained from those tests are often inconsistent because the interface regions are not directly tested. In addition, the identification of the interface dimensions (thickness) has been lacking.

2.2 Quantitative Nanoindentation

It is proposed that the quantitative nanoindentation technique be used to study the properties at the interfaces. Nanoindentation is a new method to characterize the mechanical properties of very small volumes like thin films or interfaces, coatings and

surface layers including those modified by ion implantation since the layer need not be removed from the substrate. The spatial variation of the properties can also be obtained by indentation on the scales of micro, nano and pico levels with good resolution. Employing high-resolution sensors and actuators, nanoindentation can continuously monitor the loads and displacements during loading and unloading as the indenter is driven into and withdrawn from the test material. From the load-depth curves, many quantitative information such as contact area, contact depth, stiffness, hardness, and elastic modulus are obtained. For this purpose, nanoindentation is used to characterize the characteristics at the interfaces of dissimilar materials. The nanoindentation tests will be conducted by using finite element simulation. Extensive literatures exist on the use of nanoindentation technique. The review is focused on the numerical simulation of the nanoindentation method, which is most relevant to the present research.

Numerical methods such as finite element method can be employed to simulate the nanoindentation technique to test the material properties. Bhattacharya and Nix [10], [11], Pharr and Bolshakov [12], Larsson et al [13] have used the finite element method to simulate the nanoindentation experiment to validate the use of the stiffness method for analyzing nanoindentation data.

Shih et al. [14], Cheng and Cheng [15], have used finite element simulation to evaluate the effect of the indenter tip on contact area and indentation depth. The blunt tip geometry of the so-called nano-indenter is modeled by a spherical cap of various radii and the effect of indenter tip roundness on indentation measurement was comprehensively studied.

The elastoplastic deformation during indentation is much more complex, and numerical analysis has become a major technique to study this type of indentation. Shu and Fleck [16], Sinisa, Mesarovic and Fleck [17], conducted the finite element simulation to analyze the elastic-plastic deformation under a spherical tip. Taljat et al. [18, 19],

performed finite element simulation on a wide range of materials with different elastic moduli, yield strength, strain hardening exponents, and friction coefficients. The material pile-up occurring around elastic-plastic indentation was studied.

Numerical simulations have been further used to study structures with finite size (as in the case of thin films, interfaces, etc.). King [20], Doerner et al [21], has studied the elastic properties of thin films. It was found that the substrate played an important role on the hardness of the thin films examined. The contact stresses in the indentation of coating/substrate systems were investigated by Djabella and Arnell [22], Cai [23]. Page and Hainsworth [24] simulated the indentation of thin films and found that the critical ratio of thickness is a function of the yield strength ratio of the coating to the substrate and the indenter tip radius. A more comprehensive study on layered systems was conducted by Mesarovic and Fleck [25], using finite element simulation.

Most finite element simulations of the indentation problems have been 2-dimensional, axisymmetric (Figure 2.5), which is valid for indenting structures that have homogeneous properties.

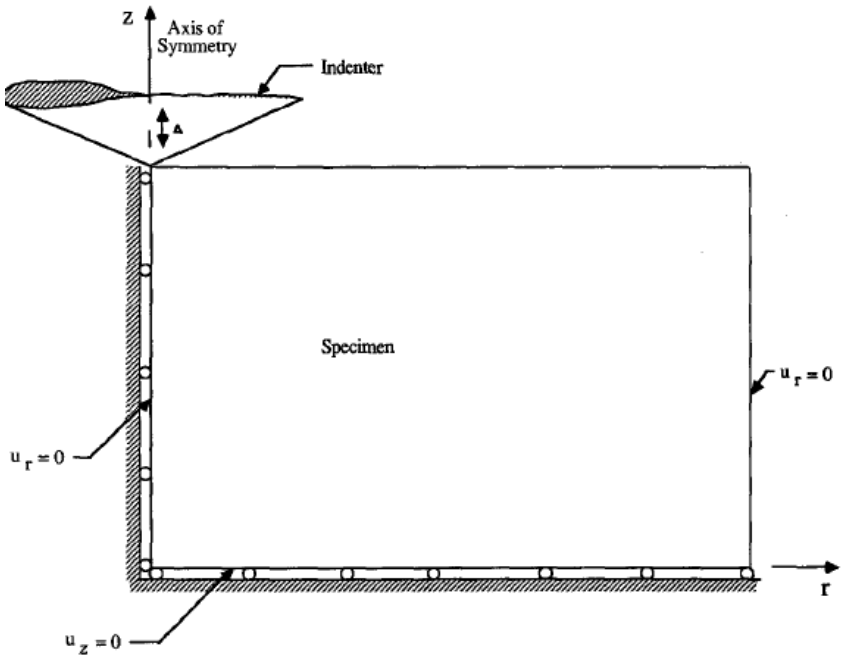

(a)

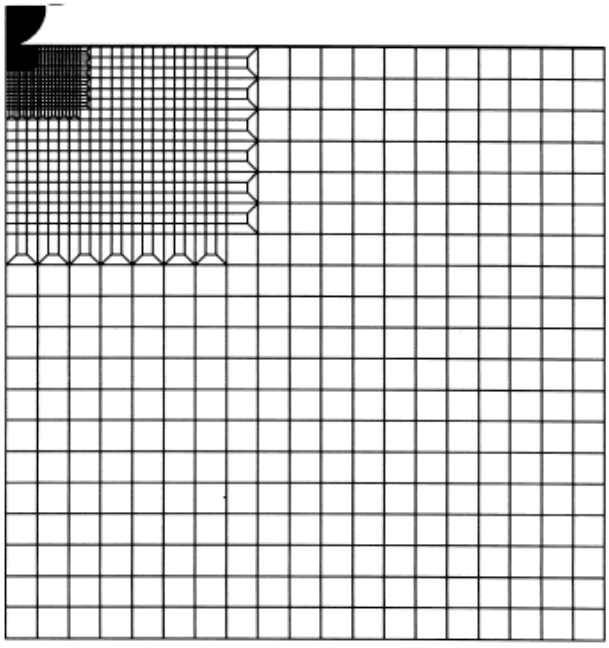

(b)

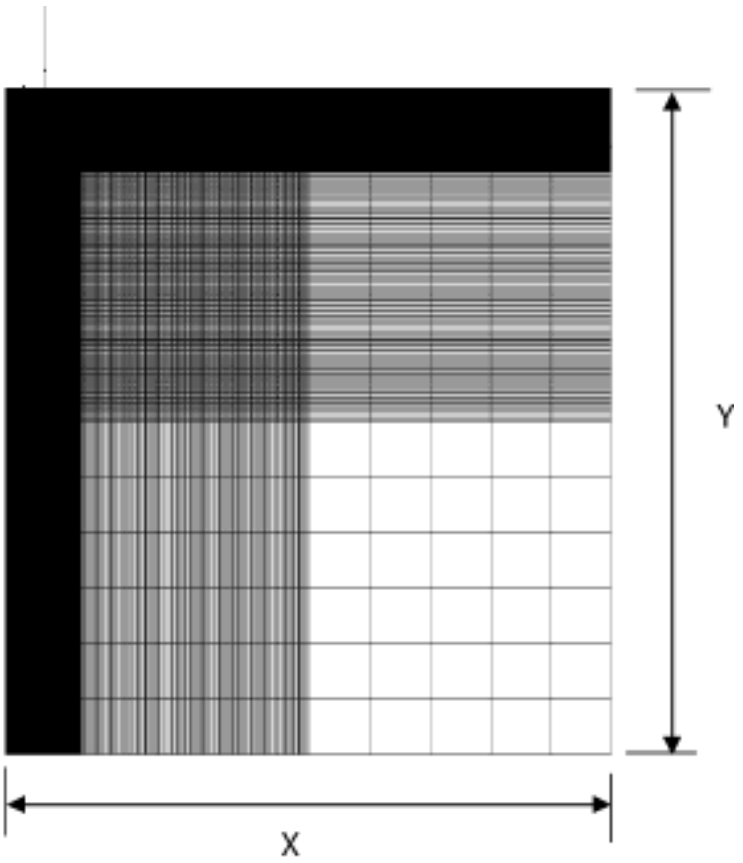

(c)

Figure 2.5 Finite element simulation of nanoindentation problems by using (a) a sharp indenter, (b) a spherical indenter, and (c) a flat indenter.

To summary, existing work has been so far limited to the examinations of mechanical properties of materials/structure in homogeneous and bi-layered structures. The proposed work is to use nanoindentation to study the interface of dissimilar materials, with the goals of both extracting mechanical properties and estimating the effective thickness of the interfaces. Three-dimensional finite element modeling will be conducted since the bimaterial structure is of heterogeneous nature.

CHAPTER 3 - GENERAL PROCEDURE OF FINITE ELEMENT MODELING

In the present work, the finite element method is used to analyze the indentation deformation at the interface of a thermo-oxidized polymer. The materials are treated as elastic-plastic and modeled by a power-law constitutive relationship between stress and strain. The indenter is assumed to be having spherical profile. The detailed procedures of the finite element modeling are presented in this chapter.

3.1 Nanoindentation as a Tool to Probe Interfaces of Dissimilar Materials

The nanoindentation method is used to probe the interface between dissimilar materials. The goals are to evaluate: 1) the mechanical properties of the interface and 2) the effective thickness of the interface. The interface could represent the region between oxidized and unoxidized polymer resins or the region between rigid fiber and polymer matrix. A general interface model can be sketched as seen in Figure 3.1. It is proposed to use a nanoindenter with spherical tip to indent across the interface region, from which quantitative information are obtained and then used to estimate the properties of the interface. The nanoindentation experiments will be conducted through the finite element simulation.

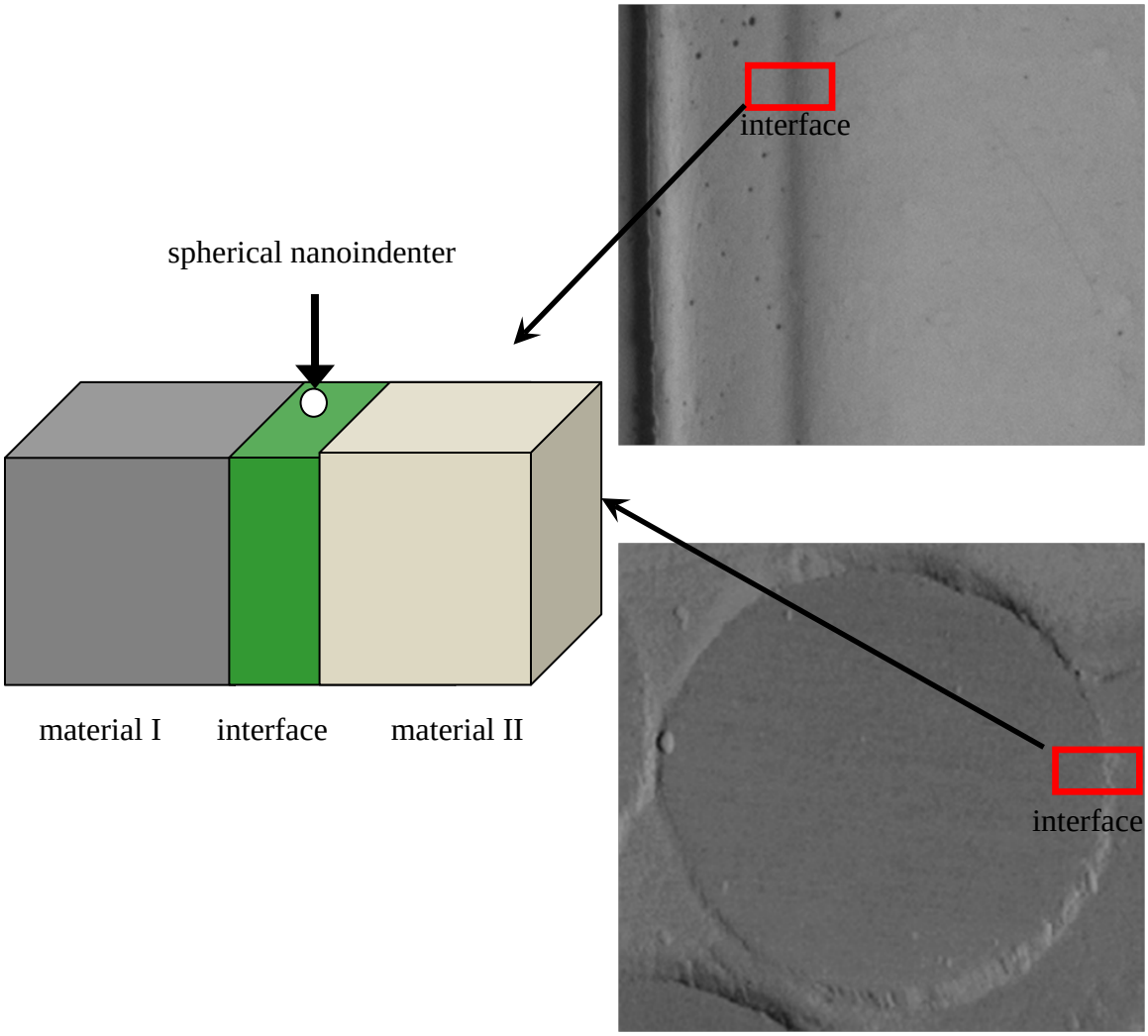

Figure 3.1 A generic model representing the interface of dissimilar materials.

3.2 Spherical Indentation as a Boundary Value Problem

The indentation at the interface of a polymer material by a spherical indenter is illustrated as see in Figure 3.2.

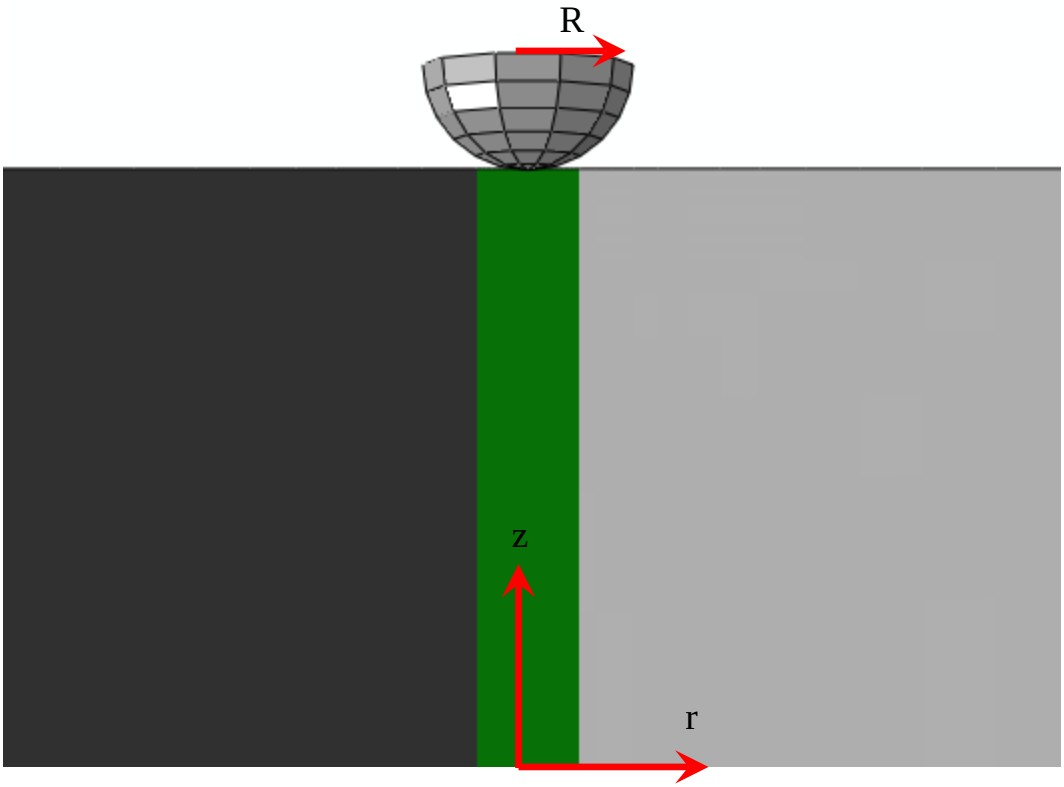

Figure 3.2 Schematic of the spherical indentation of an elastic-plastic structure.

Without any body force, the mechanical equilibrium conditions are valid during indentation,

$$\frac{\partial \sigma_{ij}}{\partial x_j} = 0 \qquad \text{----------3.1}$$

where σ_{ij} $(i, j = 1, 2, 3)$ are the components of the stress tensor and x_i are the components of the position vector of a material point.

As shown in Figure 3.2, a rigid spherical indenter is pressed onto the surface of a semi-infinite elasto-plastic material. The contact boundary conditions in a cylindrical coordinate (r, θ, z) are

$$\sigma_{rz}(r,0) = 0 \quad \text{for } r < a \qquad \text{----------3.2}$$

$$u_z(r,0) = f(r) - \delta \text{ for } r < a \qquad \text{----------3.3}$$

where σ_{rz} and σ_{zz} are respectively the shear and normal components of the stress tensor, u_z is the displacement component along the loading direction, $f(r)$ is the surface profile of the indenter tip, δ is the displacement of the indenter, and a is the radius of the contact area to be determined in the simulation.

Equation 3.2 and Equation 3.3 represent the condition of frictionless contact between the indenter and the material. Outside the contact area, the surface is at stress-free state, i.e.

$$\sigma_{rz}(r,0) = \sigma_{zz}(r,0) = 0 \text{ for } r > a \qquad \text{----------3.4}$$

The far field condition requires, $\sigma_{rz}(r,z) \to 0$, $\sigma_{zz}(r,z) \to 0$, $u_r(r,z) \to 0$, and $u_z(r,z) \to 0$ as $r \to \infty$ or $z \to -\infty$. The indentation load applied to the indenter can be calculated as

$$F = -2\pi \int_0^a \sigma_{zz}(r,0) r dr \qquad \text{----------3.5}$$

The general purpose finite element program, ABAQUS, is used for the present project. Developed by Hibbitt, Karlsson & Sorensen, Inc [26], ABAQUS is known for capable of

performing complex nonlinear simulations. The indentation procedure is assumed to be quasi-static problem, in which no time effect is considered. Hence ABAQUS-Standard is used in this work. ABAQUS process of solving usually consists of three distinct stages: preprocessing, simulation and post processing. ABAQUS-CAE is the total ABAQUS working interface that includes all the options to generate ABAQUS models, to submit and monitor jobs for analysis and also a means to review the results. In the present work, ABAQUS-CAE is used as the preprocessor of different stages of the model creation starting from the creation of Part, Property, and Assembly, defining the Step, Interaction, Load, Mesh, and generating the Job from the respective module and as the postprocessor to extract the results using Visualization module.

3.3 Finite Element Model

Due to symmetry, only half of the structure was modeled (Figure 3.3). Much of the 3D analysis is made easy with the options available in the part module of Abaqus/Standard. Once the 2D model is built, it is rather easier to either extrude, revolve or sweep about an edge or axis. As a result of which, the 3D model used in the present analysis to study the material hardness and elastic modulus was made easy since the already existing 2D model that was built in x-y plane was extruded in the z direction by the required depth.

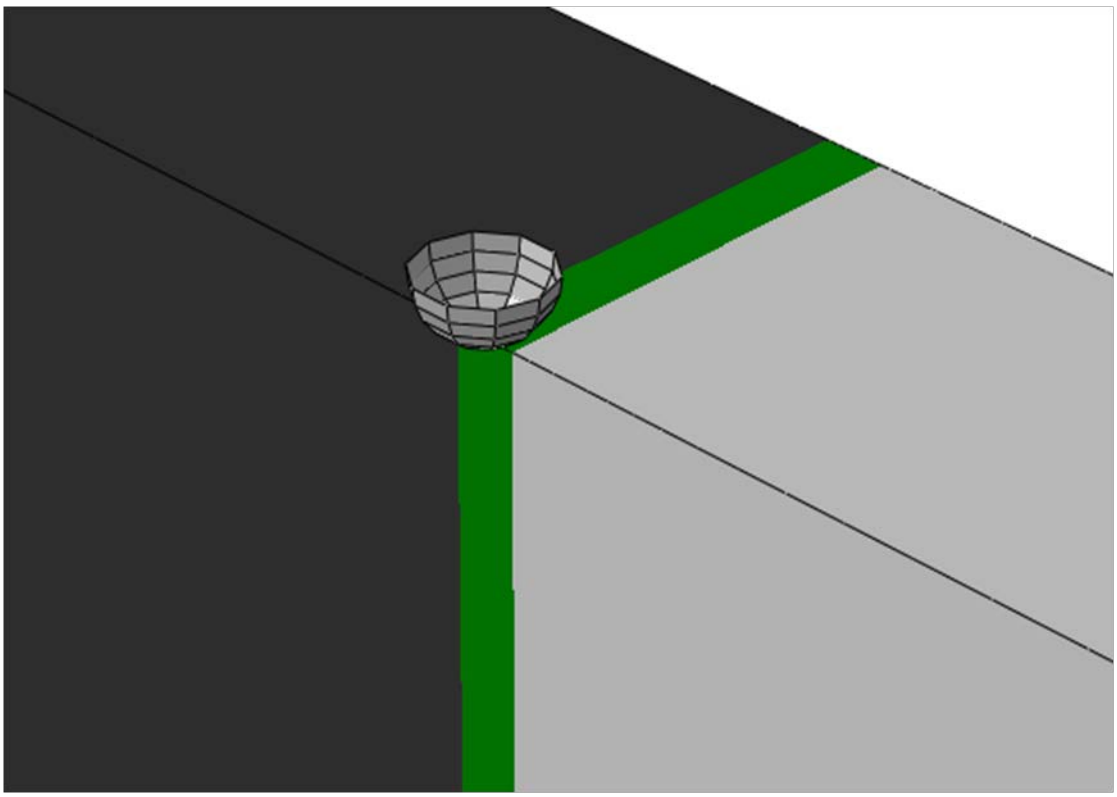

Figure 3.3 Model showing half of the structure due to symmetry.

After generating the 2D model in Abaqus-CAE the 3D model can be generated by extruding the existing 2D model in the third direction. The thickness of the extrusion was considered to be 500mm and the 3D extruded model was generated. The element type used for the analysis is C3D8R: Eight node brick element with reduced integration. "This is a general purpose linear brick element, with reduced integration (1 integration point). The shape functions are the same as for the C3D8 element" [26]. The node numbering follows the convention of Figure 3.4(a) shown below and the 2x2x2 integration point scheme in hexahedral elements is shown in Figure 3.4(b). Figure 3.4(c) shows 1x1x1 integration point scheme in hexahedral elements. Although the structure of the element is straightforward, it should not be used in the following situations:

- due to the full integration, the element will behave badly for isochoric material behavior, i.e. for high values of Poisson's coefficient or plastic behavior.
- the element tends to be too stiff in bending, e.g. for slender beams or thin plates under bending."

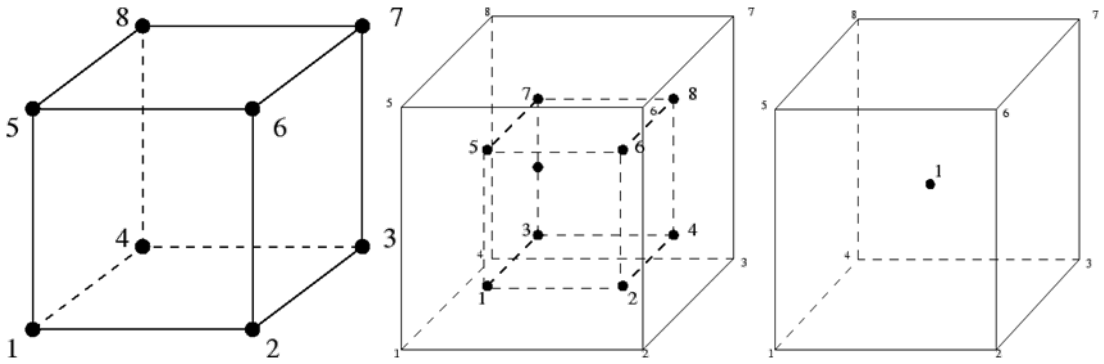

(a) (b) (c)

Figure 3.4 Sketches of C3D8 elements used in the finite element model.

Due to the reduced integration, the locking phenomena observed in the C3D8 element do not show. However, the element exhibits other shortcomings [26]:

- The element tends to be not stiff enough in bending.
- Stresses, strains are most accurate in the integration points. The integration point of the C3D8R element is located in the middle of the element. Thus, small elements are required to capture a stress concentration at the boundary of a structure.
- There are 12 spurious zero energy modes leading to massive hourglassing: this means that the correct solution is superposed by arbitrarily large displacements corresponding to the zero energy modes. Thus, the displacements are completely wrong. Since the zero energy modes do no lead to any stresses, the stress field is still correct. In practice, the C3D8R element is not very useful without hourglass control. ”

This element type was chosen as the poison’s ratio used was suitable for the present analysis and the material type and hence this avoids the bad behavior for isochoric material type. Also since fine mesh was employed in the area of interest, that made the element size to be small enough. This in turn enabled to capture proper stress concentration at the boundary of the test material although C3D8R has one integration point at the middle of the element. Due to the default hourglass control available in Abaqus C3D8R element could be used effectively in the present work.

3.4 Meshing the 3D model

Meshing is the one of the most critical and important module in the numerical methods that has a direct affect on the accuracy of the results. Depending on the type of element used the region of interest, i.e. here the interface and its immediate neighborhood the mesh needs to be designed. In the present model since the region subjected to nano-

indentation testing is the interface, a fine mesh is necessary in this region. Also since the element type used is C3D8R which requires the element size to be as less as possible in order to properly capture the stresses at the integration point that is the middle of the element, the mesh in and around the interface was made to be fine. To avoid the longer running times by the solver and to save memory the regions far away from the interface were meshed coarsely without sacrificing the accuracy of the results obtained. Figure 3.5 below the shows the meshed 3D model with proper fine mesh and coarse mesh throughout the model as required by the analysis.

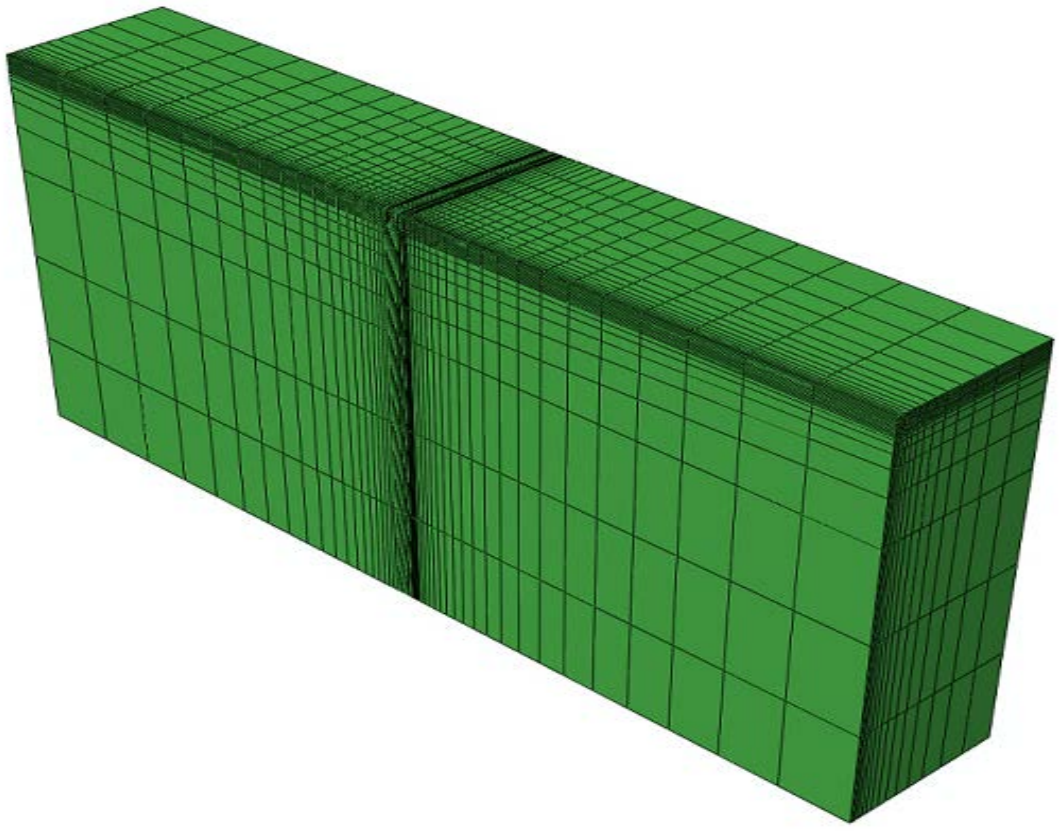

Figure 3.5 The 3D finite element model representing the layered polymer.

3.5 Boundary Conditions

As one or more degrees of freedom were to be arrested for a particular node, single point constraints (SPC), were used in the present analysis. Nodes on one face in x-y plane were completely arrested by inputting a prescribed value of zero and hence constraining any displacements in the x-y plane. Figure 3.6 shows the first boundary condition with the nodes in the x-y plane arrested to avoid the deformation in the z-direction. Figure 3.7 shows the encastre boundary condition applied to the base of the test specimen, Figure 3.8 shows the displacement boundary condition where the necessary displacement was given to the indenter to apply the load on the material, and Figure 3.9 shows the displacement boundary condition given to the reference point for the unloading step.

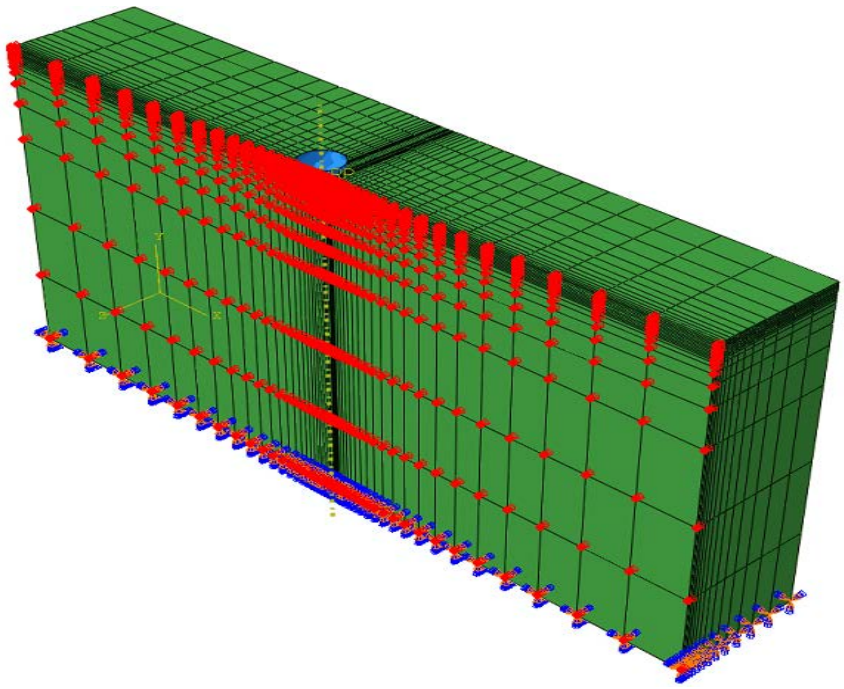

Figure 3.6 Image showing the first boundary condition with the nodes in the x-y plane arrested to avoid the deformation in the z-direction

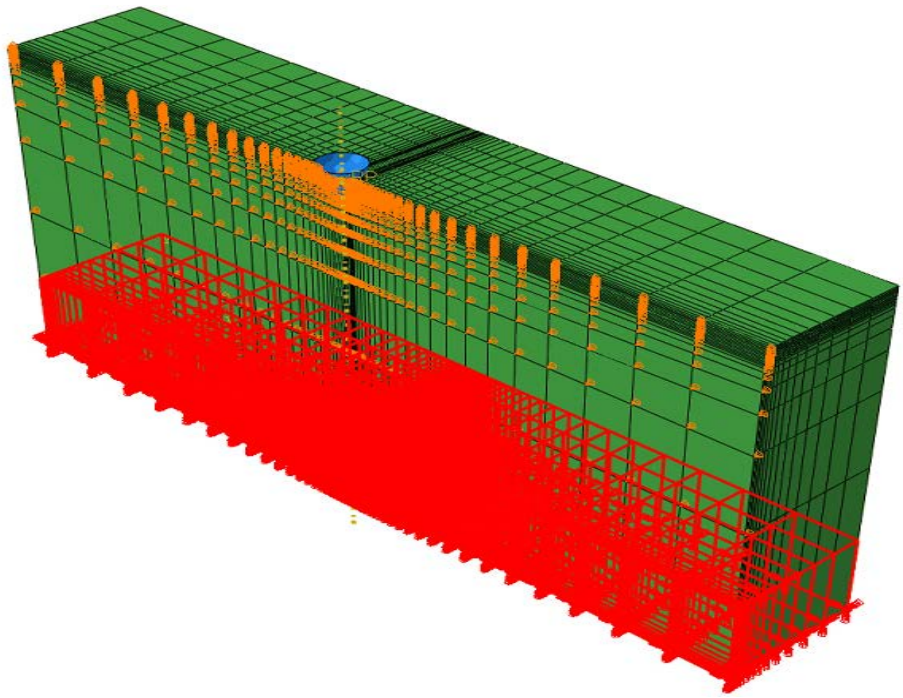

Figure 3.7 Image showing the encastre boundary condition applied to the base of the test specimen

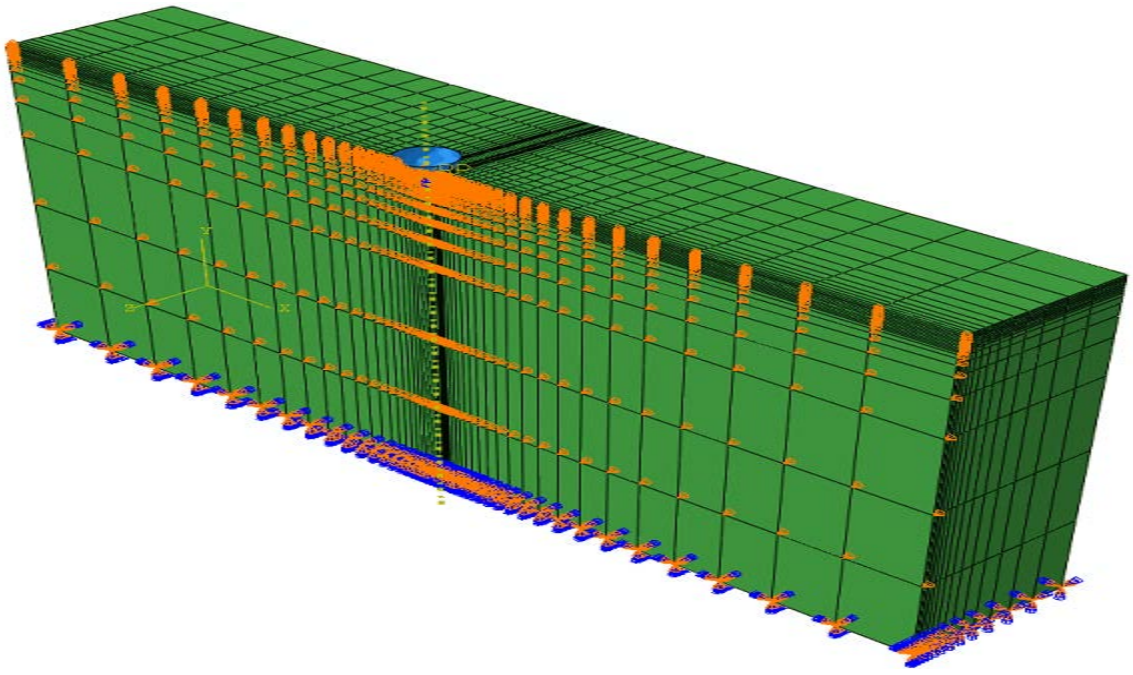

Figure 3.8 Image showing the displacement boundary condition where the necessary displacement was given to the indenter to apply the load on the material.

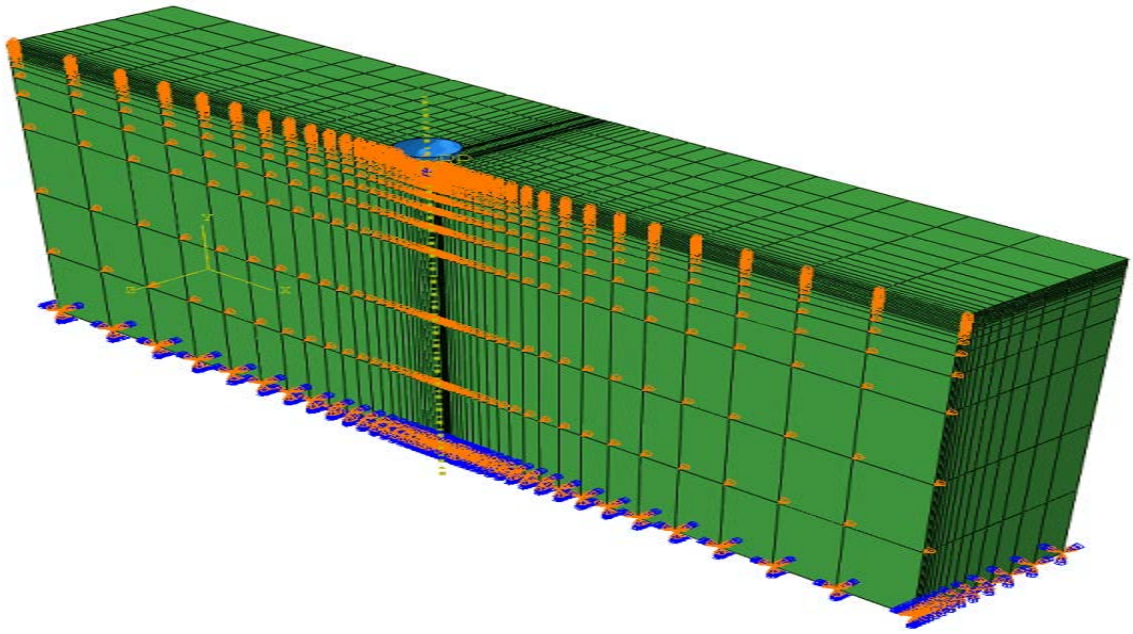

Figure 3.9 Image showing the displacement boundary condition given to the reference point for the unloading step.

3.6 Contact Interaction

Since Indentation is an example of typical contact problem, it is very important to define the contact formulation in ABAQUS. In general the interaction between contacting surfaces consists of two components: one normal to the surfaces and one tangential to the surfaces. The normal component may be referred as contact pressure and the tangential component generates the relative motion (sliding) of the surfaces involving friction. ABAQUS uses Coulomb friction model to define the interaction of contacting surfaces. The model characterizes the friction behavior between the surfaces using a coefficient of friction μ. The product μP, where P is the contact pressure between the two surfaces, gives the limiting frictional shear stress. The contact surfaces will not slip (sliding relative to each other) until the shear stress across their interface equals the limiting frictional shear stress, μP.

In our work it is assumed that the friction effect is negligible and μ=0 is defined in all the models assuming there is no slip between the surfaces in contact. The interaction between the indenter and the specimen is modeled as contact pair without any friction. According to ABAQUS user manual [26], the indenter surface is defined as the 'master' surface since the indenter is rigid body. The top of the specimen is the 'slave' surface.

3.7 Material Characteristics

3.7.1 Linear Elastic Model

Elastic deformation is observed in all the materials, when the deformation is small. For isotropic linear elastic materials, the deformation is proportional to the applied load. For a uniaxial tension state the stress-strain relationship can be expressed as

$$\sigma = E\varepsilon \qquad \text{----------3.6}$$

where ε is the uni-axial strain, σ is the uni-axial stress, and E, is the elastic modulus, the proportional coefficient also known as Young's modulus.

In three dimensional state, the stress-strain relationship of a linear elastic material can be expressed as

$$\sigma_{ij} = \frac{E}{1+\upsilon}\varepsilon_{ij} + \frac{E\upsilon}{(1+\upsilon)(1-2\upsilon)}\delta_{ij}\varepsilon_{kk} \qquad \text{----------3.7}$$

where σ_{ij} and ε_{ij} are the stress components and strain components respectively. υ is the Poisson's ratio which is a measure of transverse strain against axial strain when a uniaxial stress is applied.

3.7.2 Power Law Work Hardening Models

Once the external force applied on a material cross its elastic limit, the material will undergo plastic deformation. A power law work hardening model is accepted by most engineering materials such as metals and alloys approximately which is a material constitutive relation, the modified uniaxial stress-strain (σ-ε) curve of a stress free material can be expressed as

$$\begin{cases} \sigma = E\varepsilon & for\ \varepsilon \leq \frac{\sigma_y}{E} \\ \sigma = K\varepsilon^n & for\ \varepsilon \geq \frac{\sigma_y}{E} \end{cases} \qquad \text{----------3.8}$$

where E is elastic modulus, σ_y is yield stress, n is the work hardening exponent and K= $\sigma_y(\frac{E}{\sigma_y})^n$ is the work hardening rate. When n is zero, the above (Equation 0-3) reduces to an elastic-perfectly plastic material. To completely characterize the elasto-plastic properties of a power-law material, four independent parameters, i.e., elastic modulus E, yield stress σ_y, work-hardening exponent n, and Poisson's ratio υ, are needed. One of the major objectives of this thesis, is to relate these parameters (E, σ_y, n, υ) with the indentation responses. Since indentation induces very complicated stress and strain field beneath the indenter, FEM results obtained are useful in guiding future experiments.

To define the plastic properties of a material in ABAQUS the power law hardening material model is used, a true stress strain data spreadsheet at first is generated from the Equation 3.8. Then using the below equation, plastic strain (ε_p) is calculated.

$$\varepsilon_p = \varepsilon - \frac{\sigma_y}{E} \qquad \text{----------3.9}$$

One thing to point out is the unit system in the FEM simulation. Since the ABAQUS does not specify a unit system, the users could use a unit system arbitrarily, as long as they are in consistency in one problem. In this problem, we are considering Newton (N) for the force (load) and millimeter (mm) as the unit for the penetration (displacement). So the input mechanical properties values are to be converted to maintain the consistency of the units.

The interface problem can be sketched as seen in Figure 3.10, which consists of three distinct regions: region I made of material I, interface, and region II made of material II. The material properties at region II were fixed: E_2=1200 MPa, σ_y=59 MPa, n_2=0.5, ν=0.33. The material properties at region I were changed to various ratios, as summarized in Table 3.1. The same hardness exponent (n) was used for material I. The elastic Poisson's ratio was set to 0.33 for both materials.

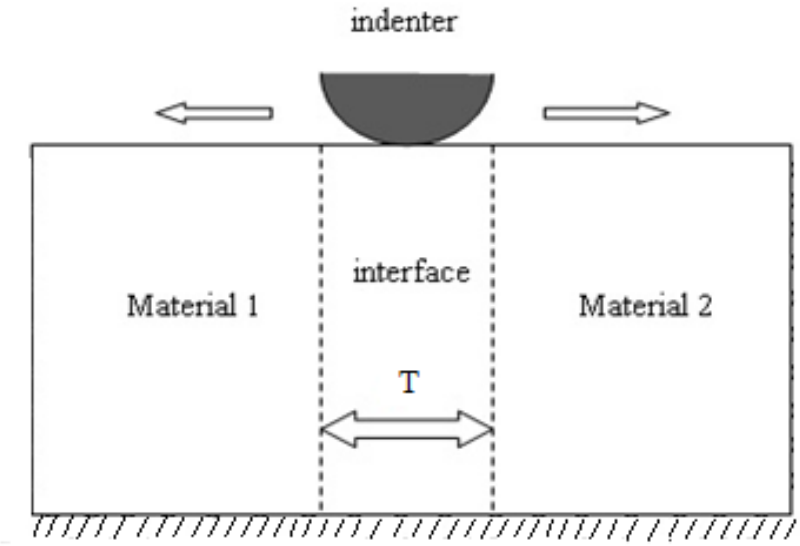

Figure 3.10 Sketch showing the interface surrounded by the bimaterial with the indenter positioned.

Table 3. 1 Material Properties Used in Finite Element Analysis.

Interface thickness, R/T	0, 0.25, 1, 2
Modulus ratio, E_1/E_2	1.5, 2, 2.5, 3, 4.175
Yield strength ratio, σ_{y1}/σ_{y2}	1.5, 2, 2.5, 3, 4.175
Hardening index, n_1, n_2	0.4, 0.5
Poisson's ratio, ν_1, ν_2	0.33

The thickness of the interface (T) was varied with respect to the indenter radius (R): T/R=0, 1, 2. The interfacial region with thickness 'T' was modeled with the properties continuously varying from region I to region II. Material interlocking was used to obtain the properties of the interface region.

3.8 Analysis Procedure

To evaluate the properties and effective thickness of the interface, a series of indentation tests were conducted with the spherical indenter along the surface of the specimen. To study the relationship between the interfacial material properties and the interfacial thickness, various scenarios were considered for the interface, including various combinations of E_1/E_2 (varied from 1.5, 2, 2.5, 3, 3.5, 4.175), σ_{y1}/σ_{y2} ((varied from 1.5, 2, 2.5, 3, 3.5, 4.175), $n_1=n_2$ (0.5, 0.4), and T/R (varied from, 0, 0.25, 1, 2). For each case, an average of 12 indents was conducted across the interface. The total indentation tests were over 1300.

The 'control displacement' method was used in the analysis. That is, a displacement was specified as input, which is equal to an indentation depth of 0.3R (R-indenter radius). For the applied displacement the reaction load (F) on the indenter was the summation of force

over the contact zone along the penetration direction. Hence the F-δ curves were obtained for each analysis, from which the mechanical properties (stiffness, hardness, and modulus) and the effective thickness of the interface were extrapolated.

CHAPTER 4 - RESULTS AND DISCUSSION

This chapter presents the results from various finite element simulations. First, the results from indentation on homogeneous material were given and then compared with the Hertz's analytical solution. That was used to validate the finite element model. Subsequently, the results from indentation on interface were presented. Various mechanical properties at the interfaces were calculated, including load-depth curves, stiffness, hardness, and modulus. The effective thickness of the interface was also estimated.

4.1 Finite Element Modeling of Homogeneous Materials

The analytical solution for the elastic indentation with a spherical tip has been derived by Hertz [27]. In the context of F-δ measurements on a flat surface (with infinite radius of curvature), which is indented by an elastic sphere, Hertz showed that:

$$F = C\delta^{\frac{3}{2}} \qquad \text{----------4.1}$$

$$C = \frac{2\sqrt{2}}{3}\mathrm{E}D^{\frac{1}{2}} \qquad \text{----------4.2}$$

where D is the diameter of the sphere and E is the reduced Young's modulus of the specimen indenter system. Assuming spherical indenter to be perfectly rigid the above equation for the force reduces to

$$F = \frac{2\sqrt{2}}{3}\frac{E\sqrt{D}}{1-\nu^2}\delta^{\frac{3}{2}} \qquad \text{----------4.3}$$

With Hertz's analytical solution, the finite element models can be validated. By using the elastic input (E=5010 MPa and ν=0.33) in the FE model, the indentation load-depth response is obtained, as shown in Figure 4.1. It can be noticed from Figure 4.1 that, for the elastic problem, the finite element solution agrees exactly with the Hertz solution. Thus, it can be concluded that the present finite element model (mesh, element sizes, boundary conditions, etc.) is valid for simulating the indentation of a half-space by a rigid sphere.

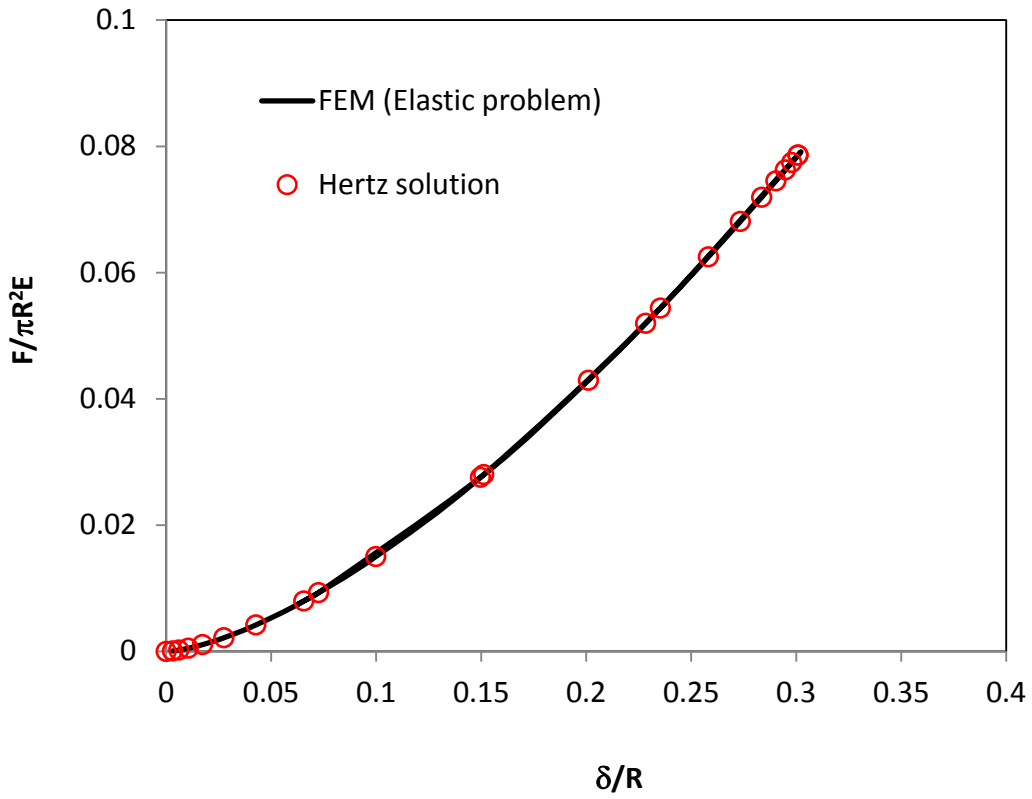

Figure 4.1 Comparison of Reaction Force from FEM Models and Hertz Model for Spherical Indenter

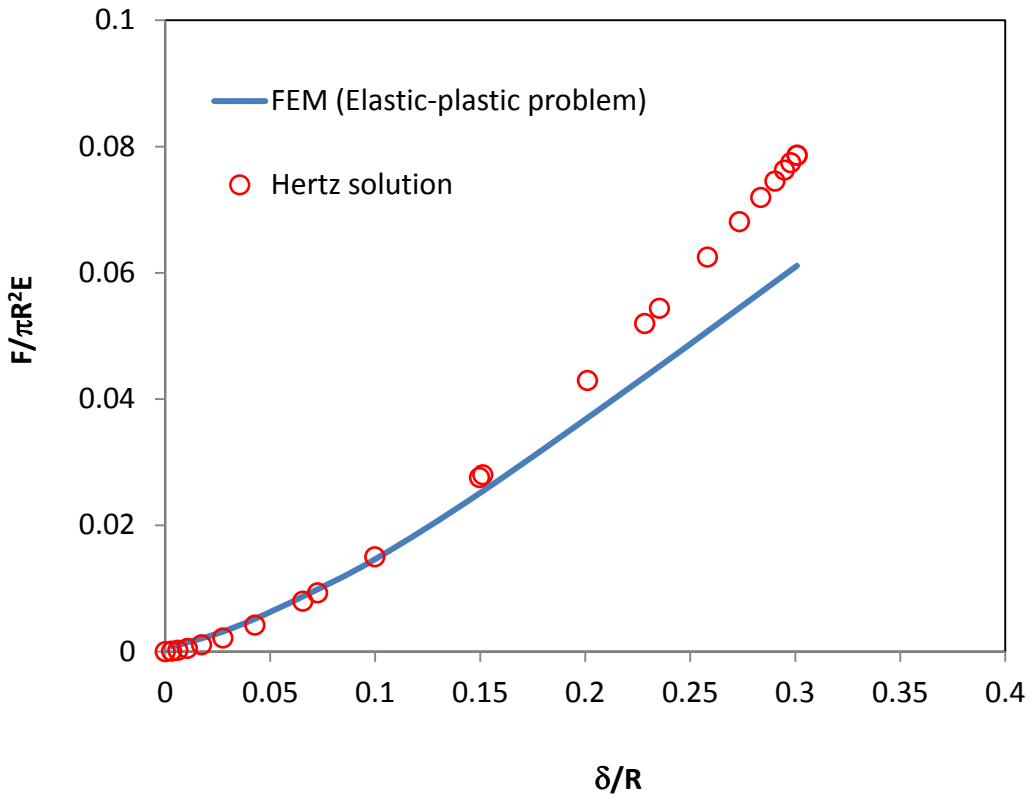

Figure 4.2 Comparison of Reaction Force from FEM Models and Hertz Model for Spherical Indenter

When the plastic definition is presented (E=5010 MPa, ν=0.33, n=0.5 in the power law model), it is seen that the Hertz's solution can only predict well the small deformation (δ/R<10%) and then become invalid at large displacements (Figure 4.2). This indicates that the Hertz solution cannot be used to model the elastic-plastic problems.

To validate the elastic-plastic finite element model, the indentations on homogeneous materials are performed first. A range of known materials are tested and the moduli are calculated from the indentation load-depth responses. The procedures for analyzing nanoindentation experiment have been well established. As an indenter is driven into and withdrawn from the testing material, the resultant load-displacement curve can be recorded continuously, as shown in Figure 4.3. It is assumed that during the initial

unloading the deformation is purely elastic [28], thus, the slope of the initial portion of the unloading curve yields the elastic contact stiffness, *S*:

$$S = dP/dh \qquad \text{----------4.5}$$

Where *P* is the load and *h* is the displacement at the indenter tip.

Following Oliver and Pharr [29, 30], the contact depth, h_c, can be further determined from the loading-unloading curve:

$$h_c = h - 0.75P/S, \qquad \text{----------4.6}$$

Where *h* is the total indentation depth and *P* the maximum load.

Using the contact depth, the projected contact area, A, can be estimated through the impression radius a:

$$A = \pi a^2 \qquad \text{----------4.7}$$

The indenter-sample contact radius (a) is then computed via the standard procedure

$$a = \sqrt{2h_c R - h_c^2} \qquad \text{----------4.8}$$

Once the contact area is determined the hardness and reduced modulus and can be calculated as:

$$H = P/A \qquad \text{----------4.9}$$

$$E = \frac{1-\nu^2}{\frac{1}{E_r} - \frac{1-\nu_i^2}{E_i}} \qquad \text{---------- 4.10}$$

where $E_r = \frac{\sqrt{\pi}}{2}\frac{S}{\sqrt{\pi a^2}}$. E_i and ν_i are the elastic modulus and Poisson's ratio of the indenter (for diamond indenter: E_i=1140 GPa and ν=0.07).

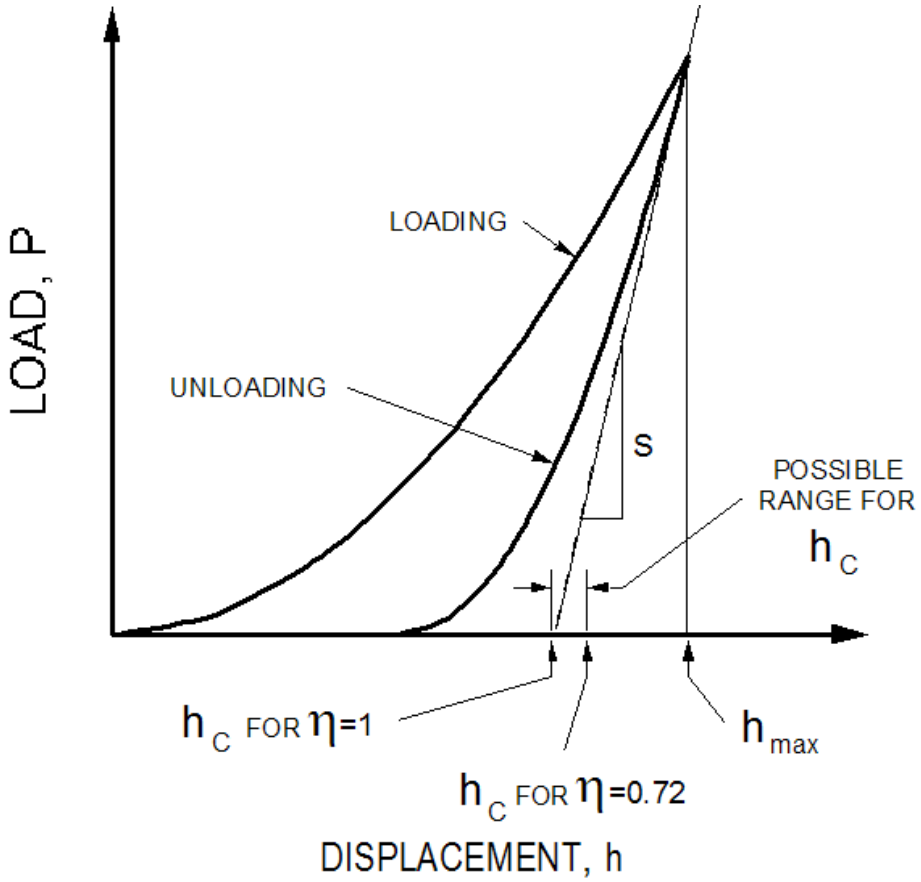

Figure 4.3 Schematic of typical load-displacement data defining key experimental quantities.

Figure 4.4 shows the indentation load-depth curves of various homogeneous materials with known modulus (E=1020~5010 MPa). Based upon the information obtained from the load-depth curves (stiffness S, contact depth d, maximum load P), the modulus of each material is extracted by using Equation 4.10. A comparison of modulus from

indentation tests and the given values is shown in Figure 4.5. It is seen that the results from indentation tests agrees well with the input values, with a error less than 7%. This indicates that the present elastic-plastic FE model is appropriate for studying the interface problems.

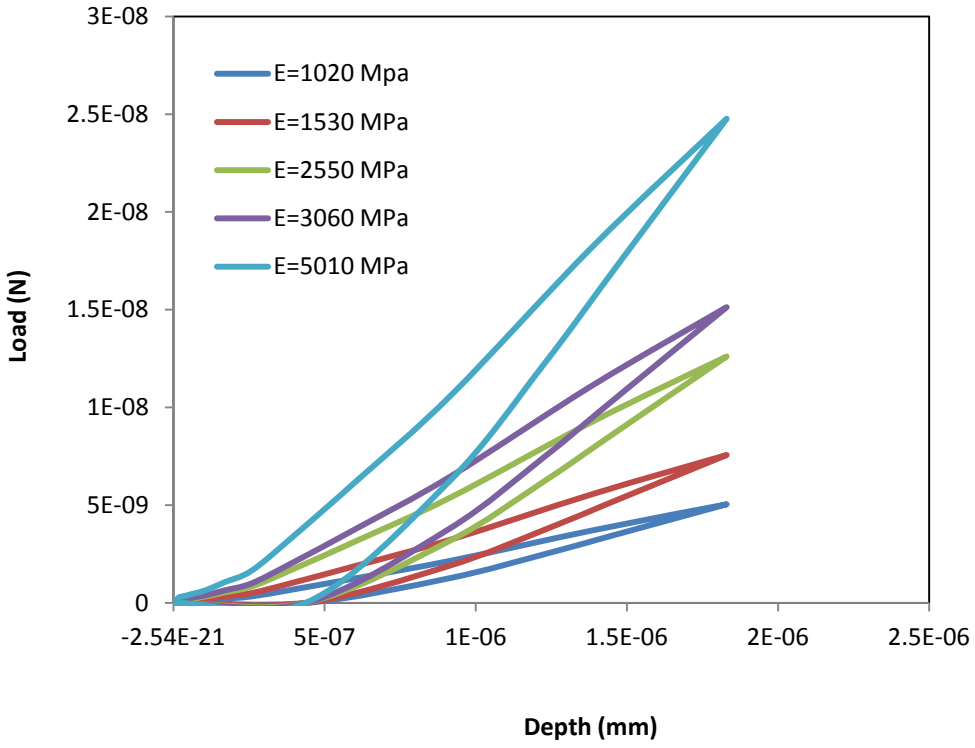

Figure 4.4 Indentation load-depth curves of homogeneous materials.

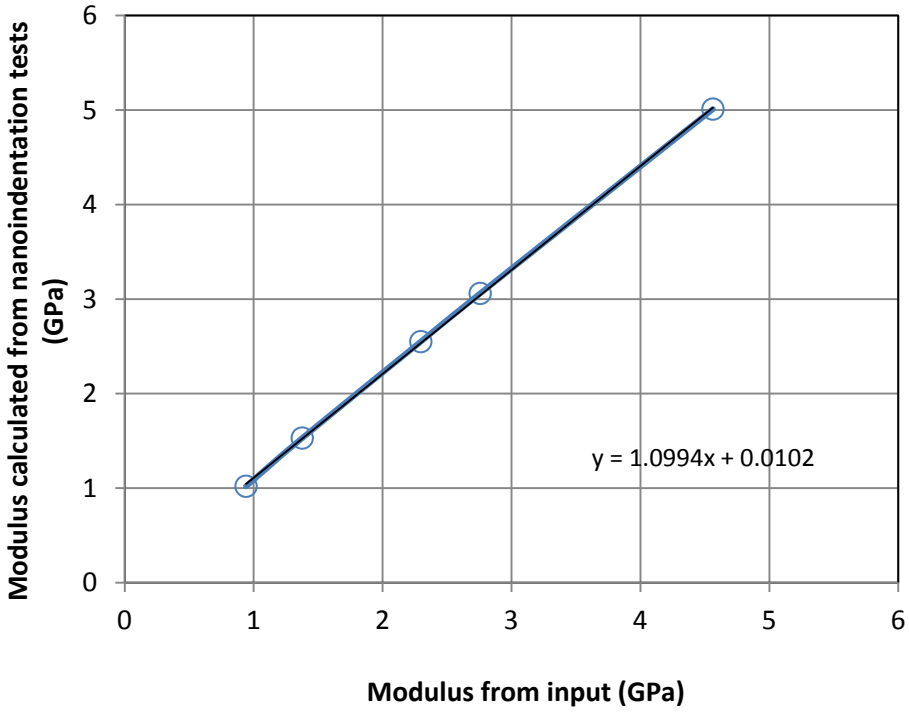

Figure 4.5 Comparison of modulus from indentation tests and input values for a variety of homogeneous materials.

4.2 Stress Distribution at the Interface

The contours of von Mises stress, σ_{Mises}, at the peak displacement are shown in Figure 4.6 at different positions for a given set of material properties: $E_1/E_2=3$, $R/T=0.25$, $n_1=n_2=0.5$. At positions far away from the interface, the materials are essentially homogeneous and thus the von Mises contours are continuous and not affected by the presence of the interface. Within the interface, the materials are inhomogeneous and the resultant von Mises contours are seen to be discontinuous.

Figures 4.6-4.8 show the contours of von Mises at peak displacement at the center of the interface for different modulus ratios: $E_1/E_2=1.5\sim4.175$. It is seen that as the stress

distributions within the interface are strongly affected by the modulus of the bulk materials. The higher the modulus ratio, the more irregular of the stress trajectory is.

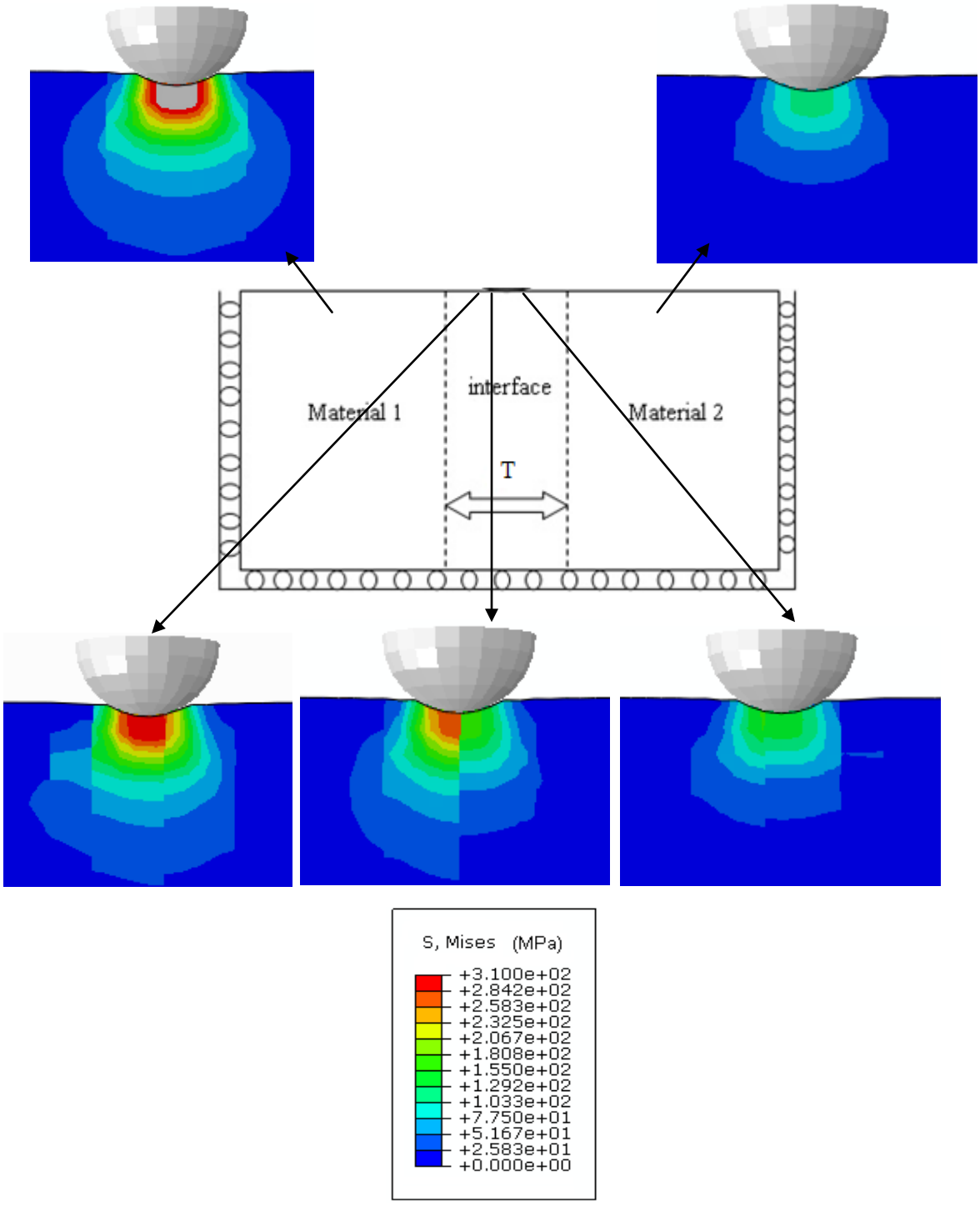

Figure 4.6 von Mises stress distribution across the interface for E_1/E_2=3 and R/T = 0.25.

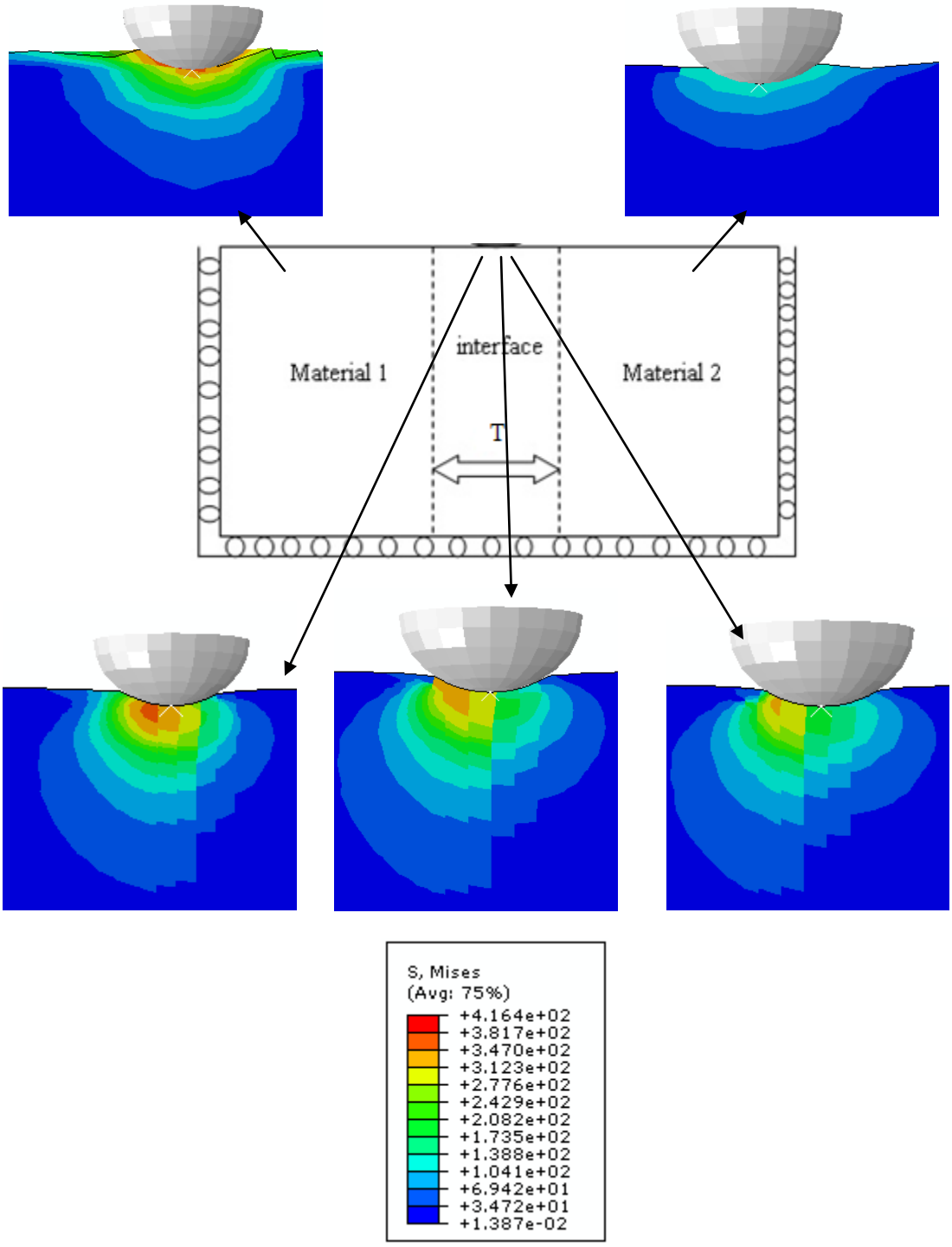

Figure 4.7 von Mises stress distribution across the interface for $E_1/E_2 = 3$ and $R/T = 1$.

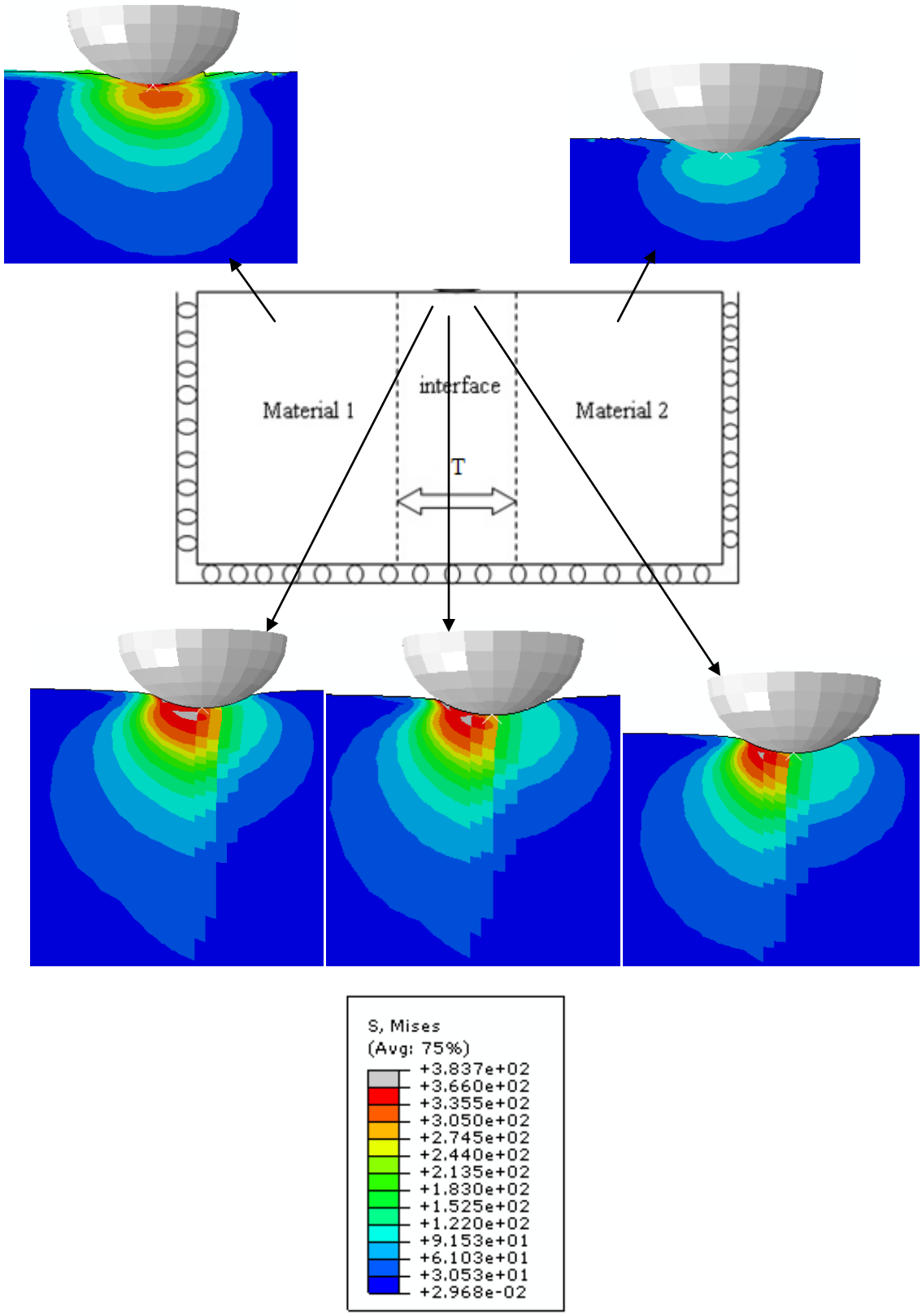

Figure 4.8 von Mises stress distribution across the interface for E_1/E_2=3 and R/T = 2.

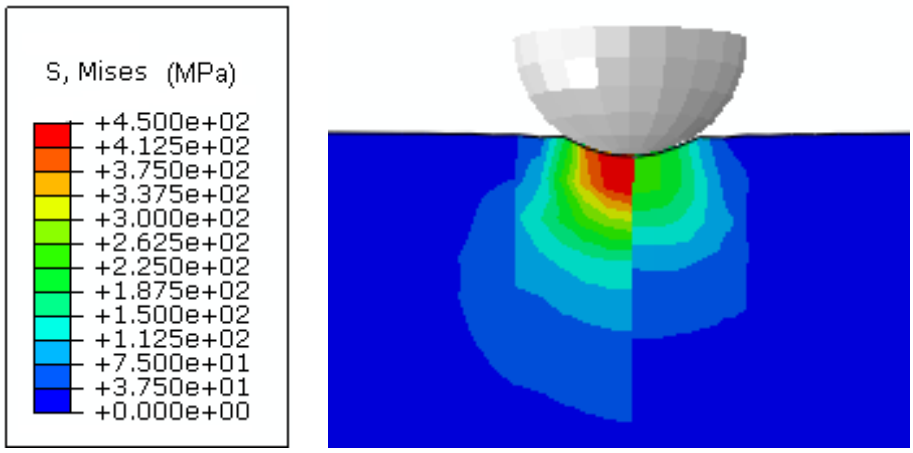

Figure 4.9 von Mises stress distribution at the interface: R/T=0.25, E_1=5010 MPa, E_2=1200 MPa

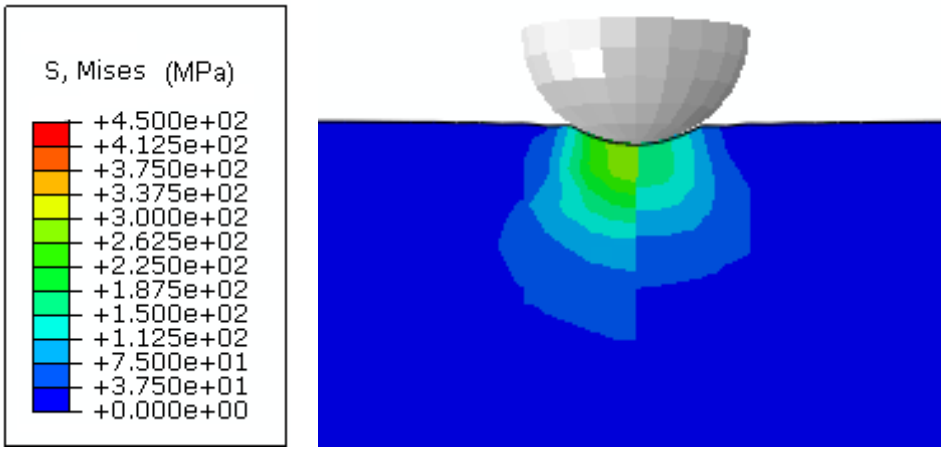

Figure 4.10 von Mises stress distribution at the interface: R/T=0.25, E_1=4534 MPa, E_2=1200 MPa

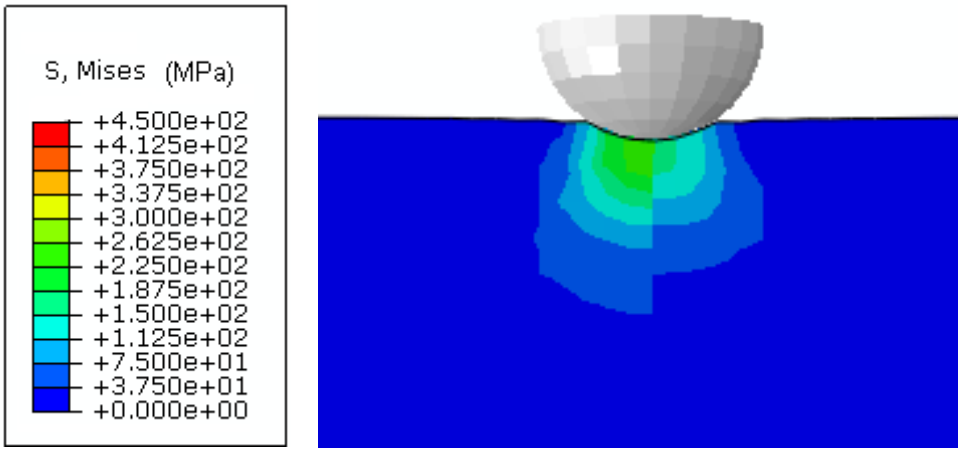

Figure 4.11 von Mises stress distribution at the interface: R/T=0.25, E_1=4058 MPa, E_2=1200 MPa

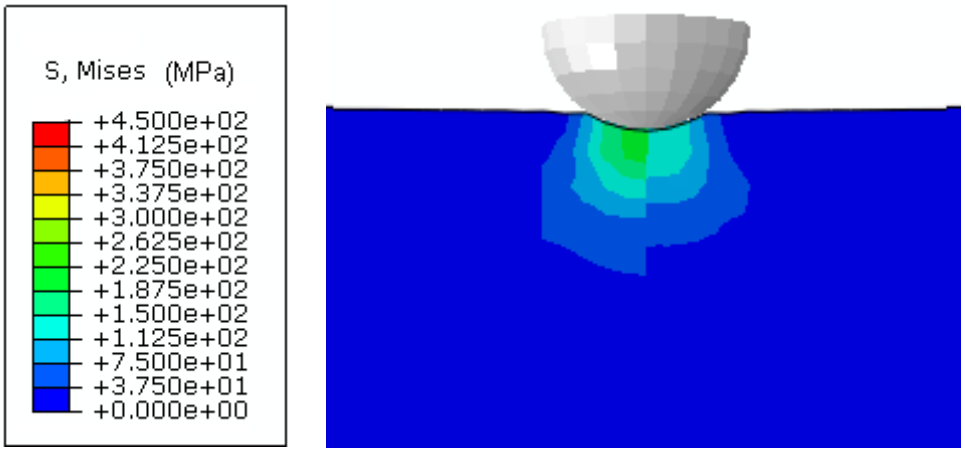

Figure 4.12 von Mises stress distribution at the interface: R/T=0.25, E_1=2153 MPa, E_2=1200 MPa

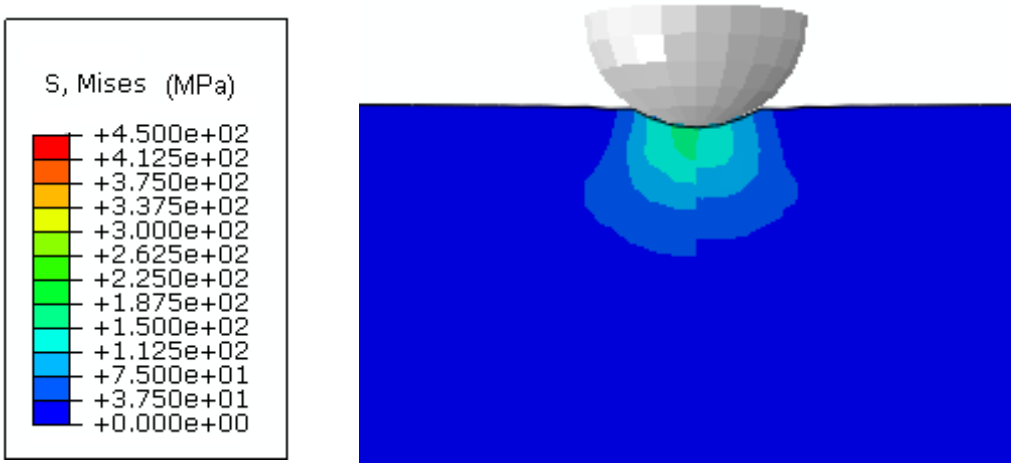

Figure 4.13 von Mises stress distribution at the interface: R/T=0.25, E_1=1676 MPa, E_2=1200 MPa

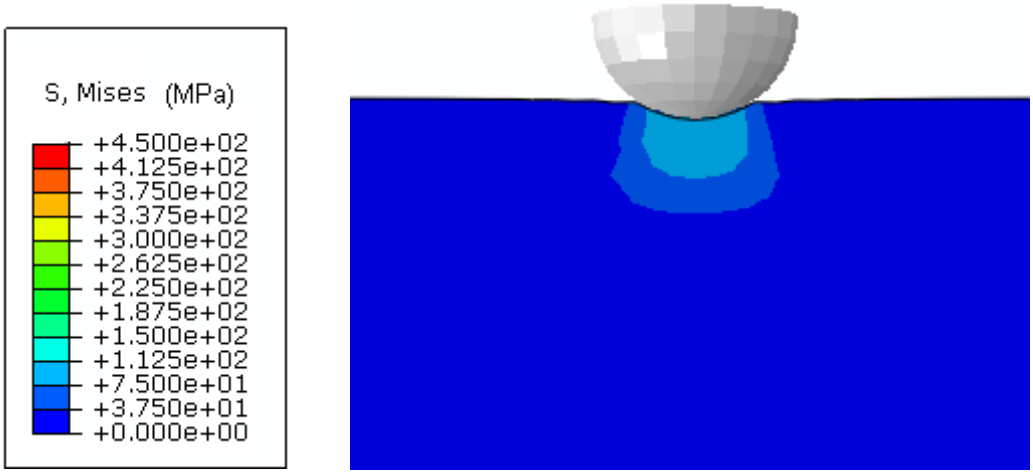

Figure 4.14 von Mises stress distribution at the interface: R/T=0.25, E_1=1200 MPa, E_2=1200 MPa

4.3 Mechanical Properties of the Interface

The nanoindentation tests are conducted at positions across the interfaces, as sketched in Figure 3.2. The indentation load depths curves across the interfaces are obtained, as shown in Figures 4.15-4.17. At locations far away from the interfaces, the materials are essentially homogeneous, representing the hardest and softest material, respectively. Within the interfaces, the materials have varying properties, resulting in progressively lower indentation loads.

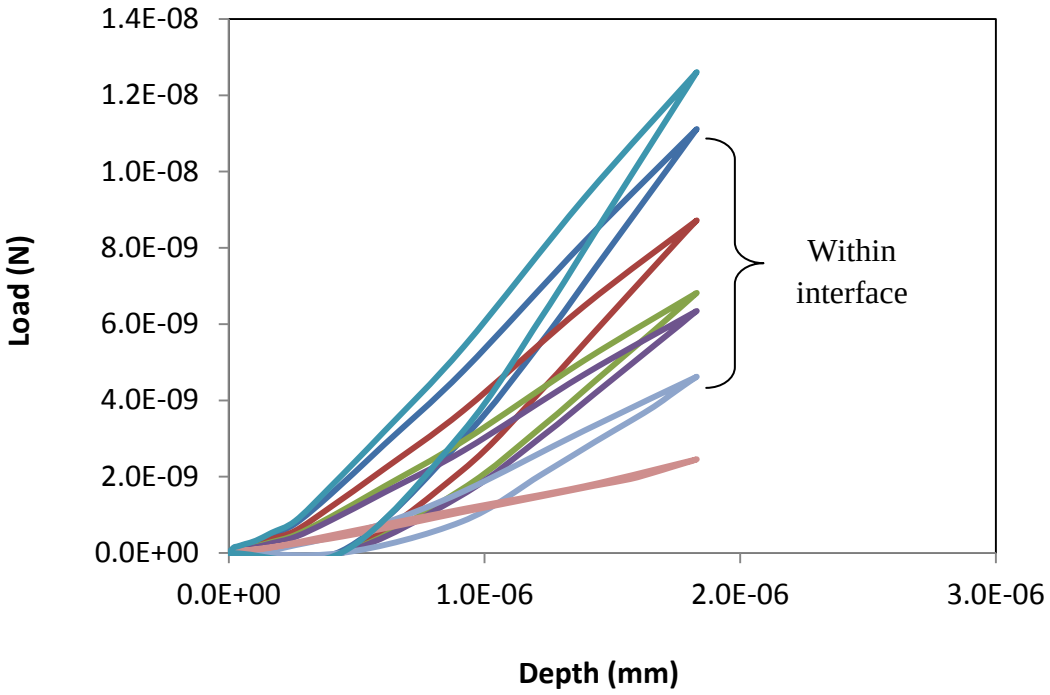

Figure 4.15 Indentation load-depth curves across the interface: E_1/E_2=2.5, R/T=0.5.

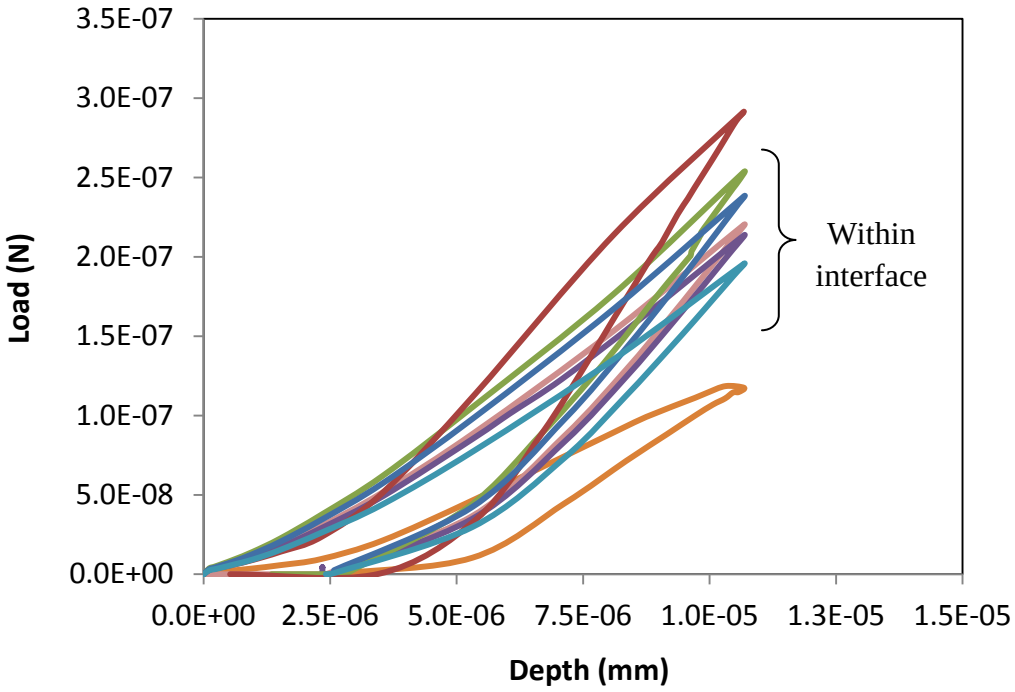

Figure 4.16 Indentation load-depth curves across the interface: E_1/E_2=2.5, R/T=1.

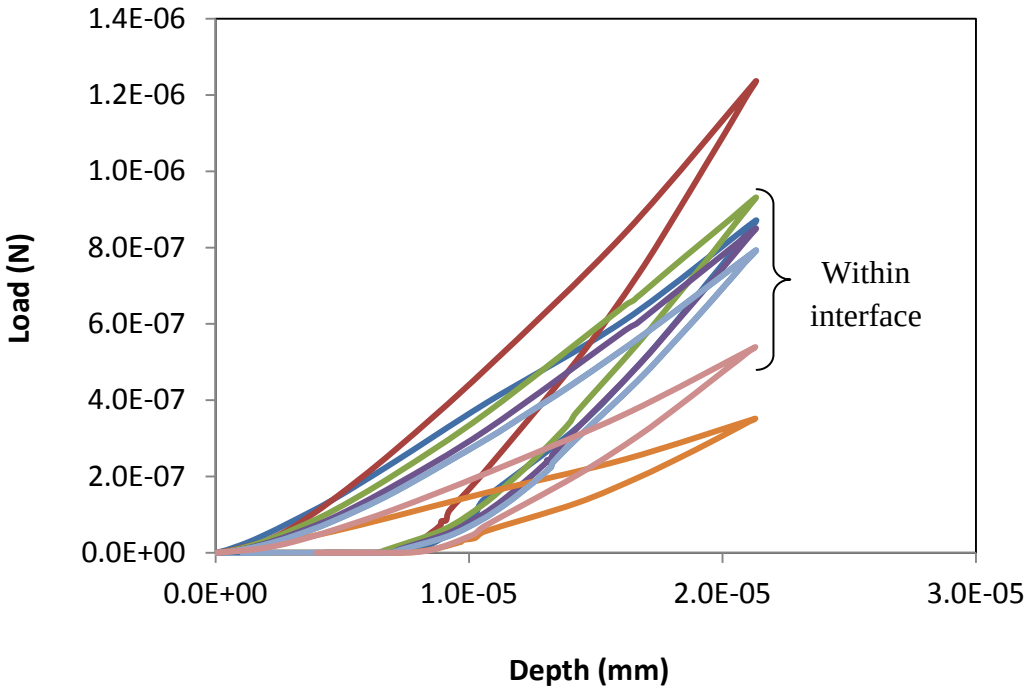

Figure 4.17 Indentation load-depth curves across the interface: E_1/E_2=2.5, R/T=2.

By analysing the load-depth curves, the materials properties (S, H, E) across the interfaces can be calculated by using Equations 4.5-4.10. Figures 4.18-4.26 show the plots for material properties vs position with different interface thickness: R/T=0, 1, and 2.

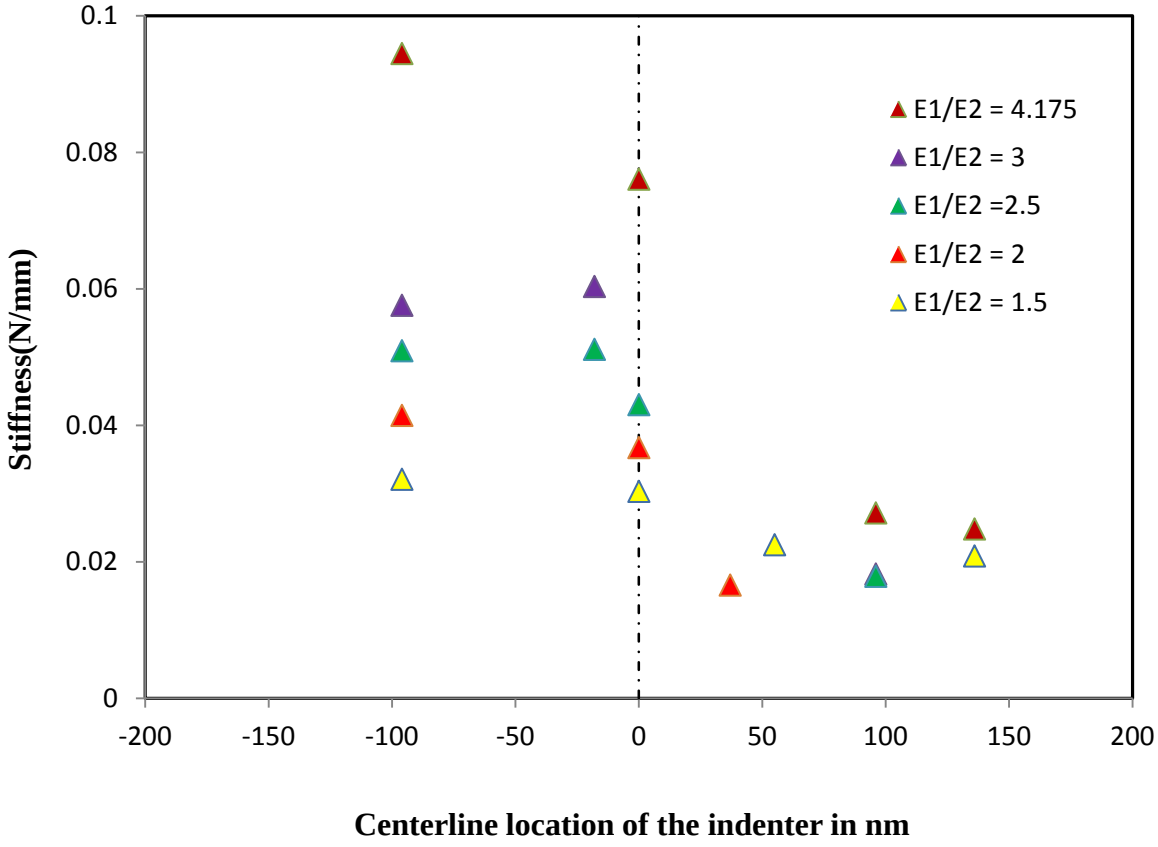

Figure 4.18 Stiffness vs. position across the interface: R/T=0. Dashed lines indicate the boundaries of the interface.

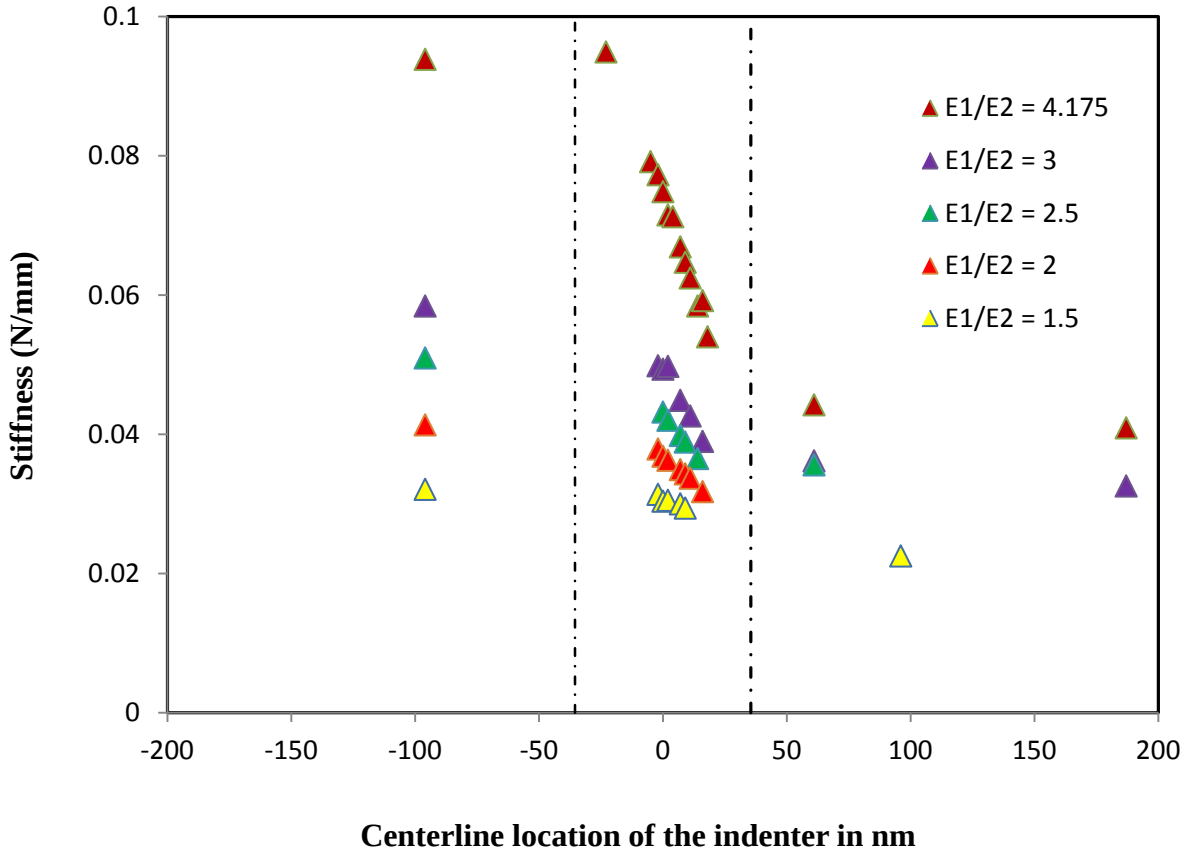

Figure 4.19 Stiffness vs. position across the interface: R/T=1. Dashed lines indicate the boundaries of the interface.

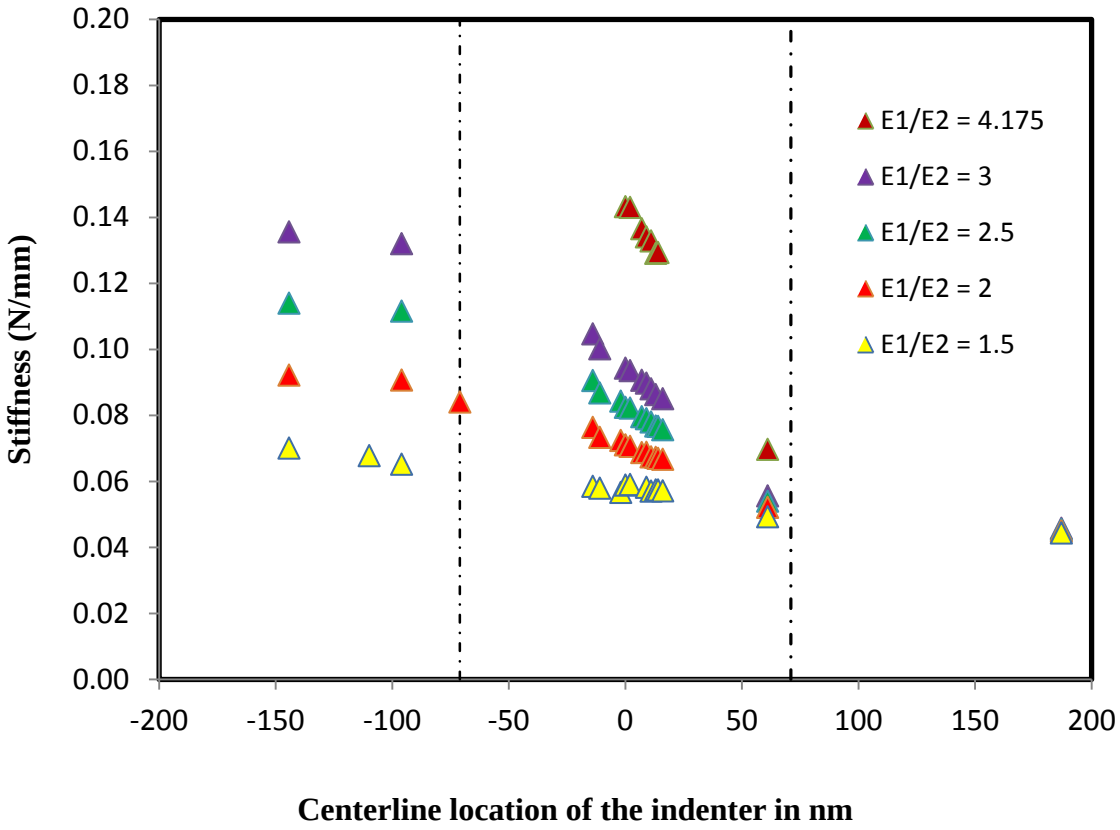

Figure 4.20 Stiffness vs. position across the interface: R/T=2. Dashed lines indicate the boundaries of the interface.

Table 4.3. 1 Shows the comparison of stiffness in the interface region for different ratios of elastic modulus of the oxidized to unoxidized regions and for different cases of R/T.

Stiffness in the interface (N/mm)			
E_1/E_2	R/T=0	R/T=1	R/T=2
1.5	0.030331	0.030394	0.058906
2	0.03674	0.036846	0.071094
2.5	0.043035	0.043197	0.082459
3	0.060348	0.049354	0.094337
4.175	0.076073	0.074854	0.143271

From the table above it can be seen that the stiffness in the interface region increased as the radius of the indenter is increased relative to the interface thickness for each modulus ratio ranging from 1.5 to 4.175.

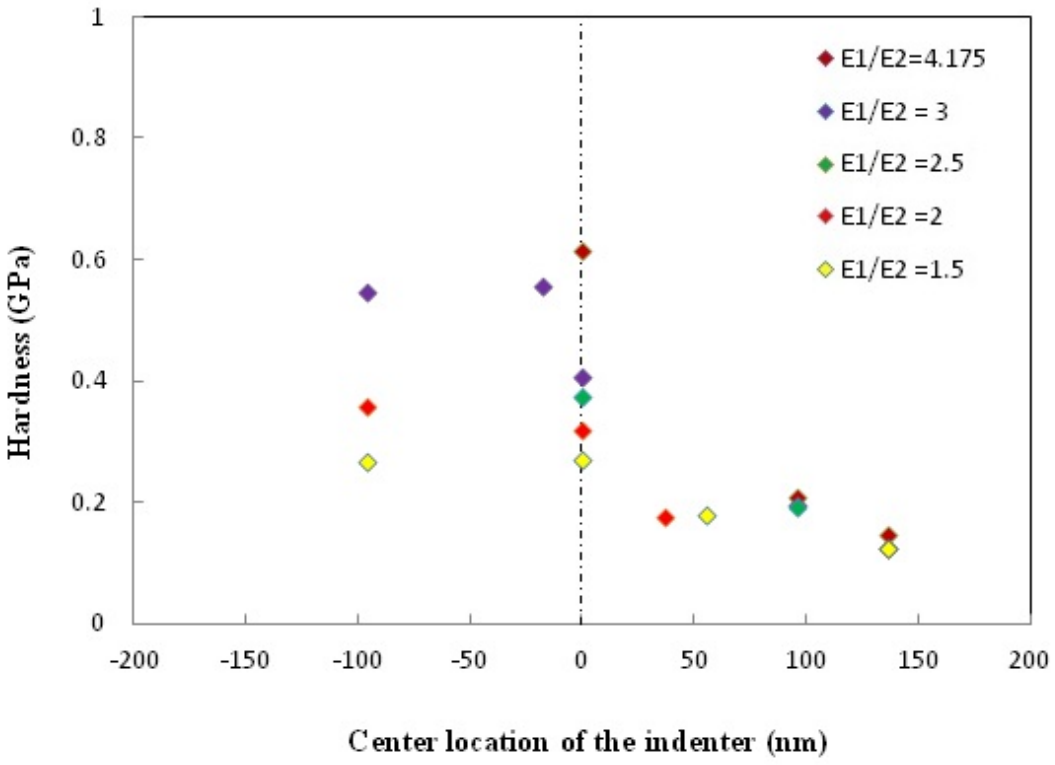

Figure 4.21 Hardness vs. position across the interface: R/T=0. Dashed lines indicate the boundaries of the interface.

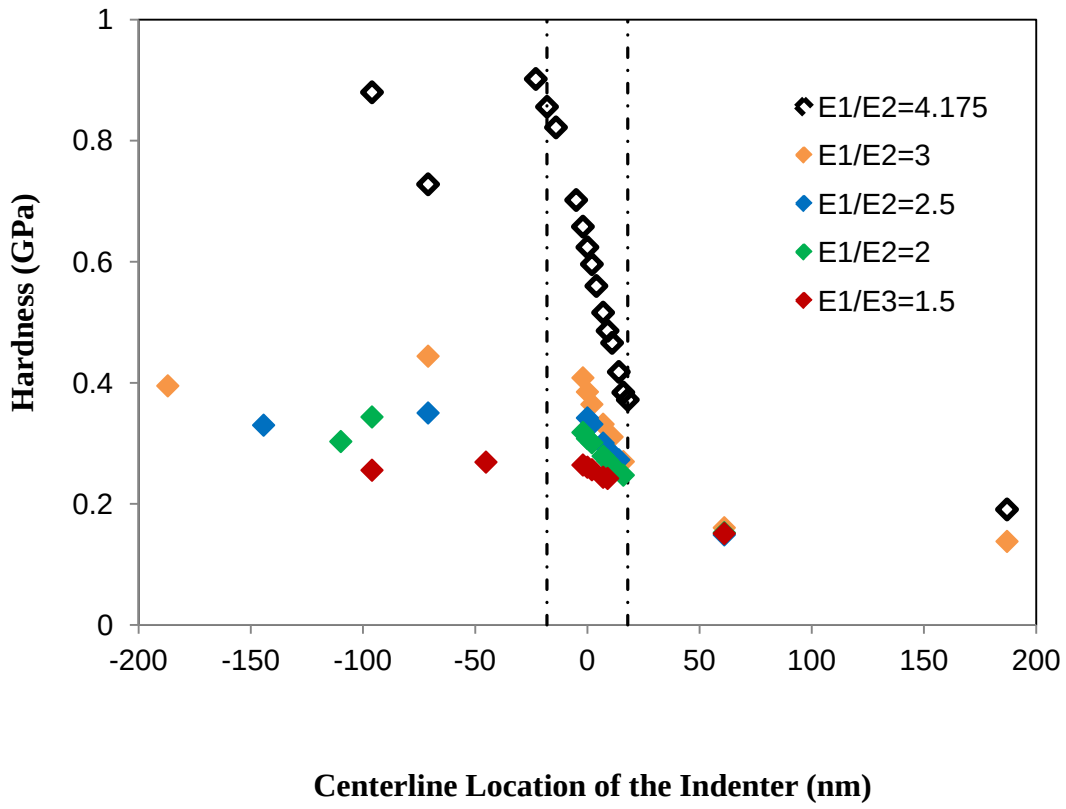

Figure 4.22 Hardness vs. position across the interface: R/T=1. Dashed lines indicate the boundaries of the interface.

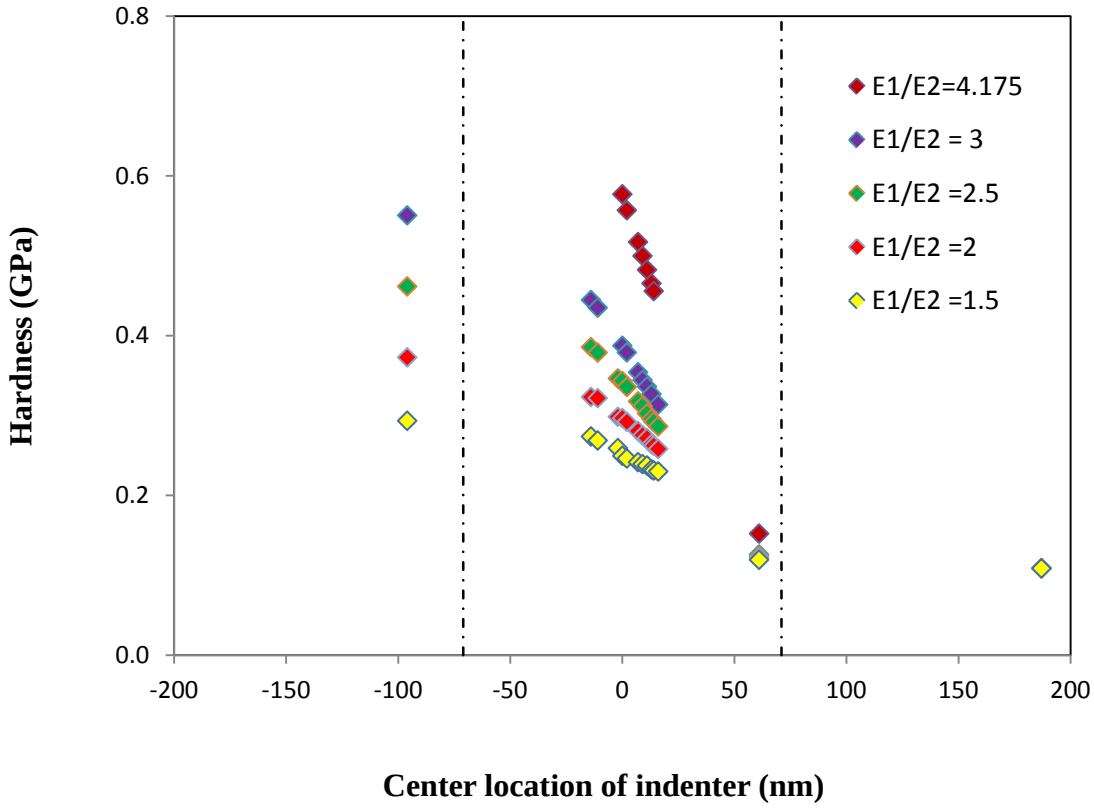

Figure 4.23 Hardness vs. position across the interface: R/T=2. Dashed lines indicate the boundaries of the interface.

Table 4.3. 2 Shows the comparison of hardness in the interface region for different ratios of elastic modulus of the oxidized to unoxidized regions and for different cases of R/T.

Hardness in the interface (GPa)			
E_1/E_2	R/T=0	R/T=1	R/T=2
1.5	0.1354	0.1303	0.1248
2	0.1597	0.154	0.1484
2.5	0.1876	0.171	0.1716
3	0.2775	0.1925	0.1937
4.175	0.3069	0.312	0.2885

From the values of hardness in the table it can be seen that the hardness has increased as the ratio of elastic modulus of oxidized to un-oxidized regions increased. And also with the increase in the radius of the indenter relative to the interface thickness, hardness has consistently remained the same or decreased for different modulus ratios.

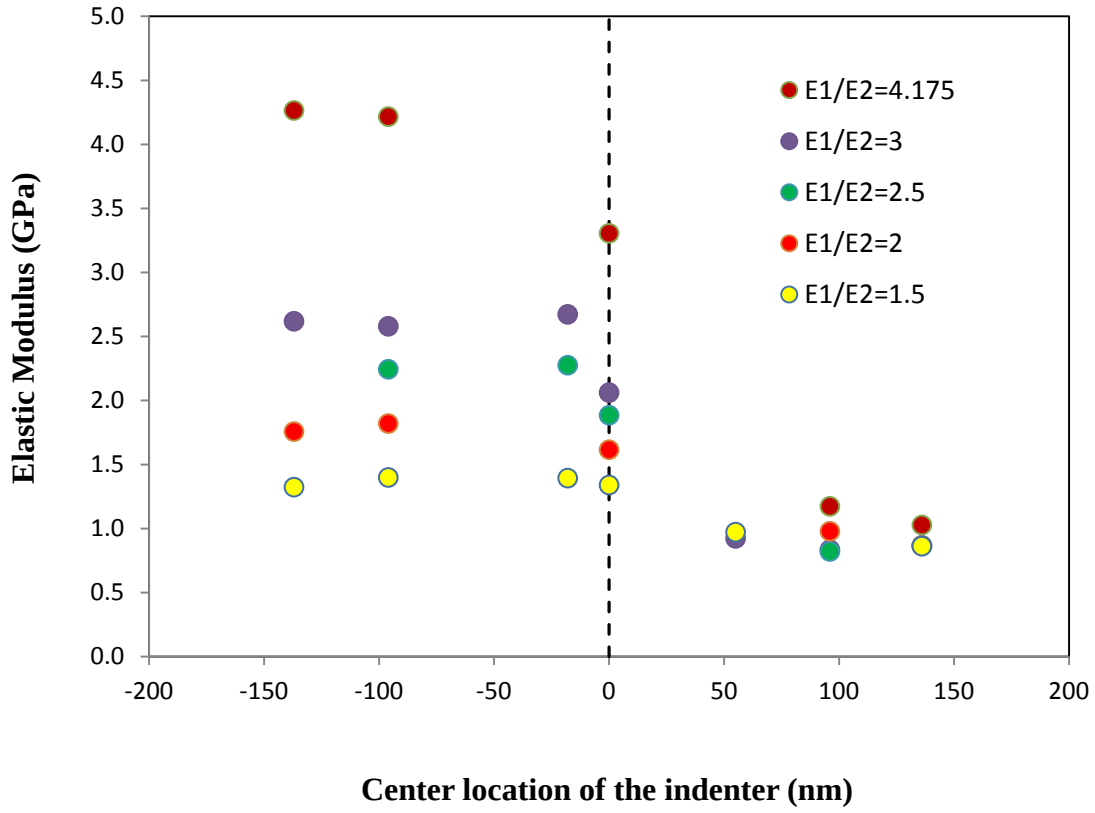

Figure 4.24 Modulus vs. position across the interface: R/T=0. Dashed lines indicate the boundaries of the interface.

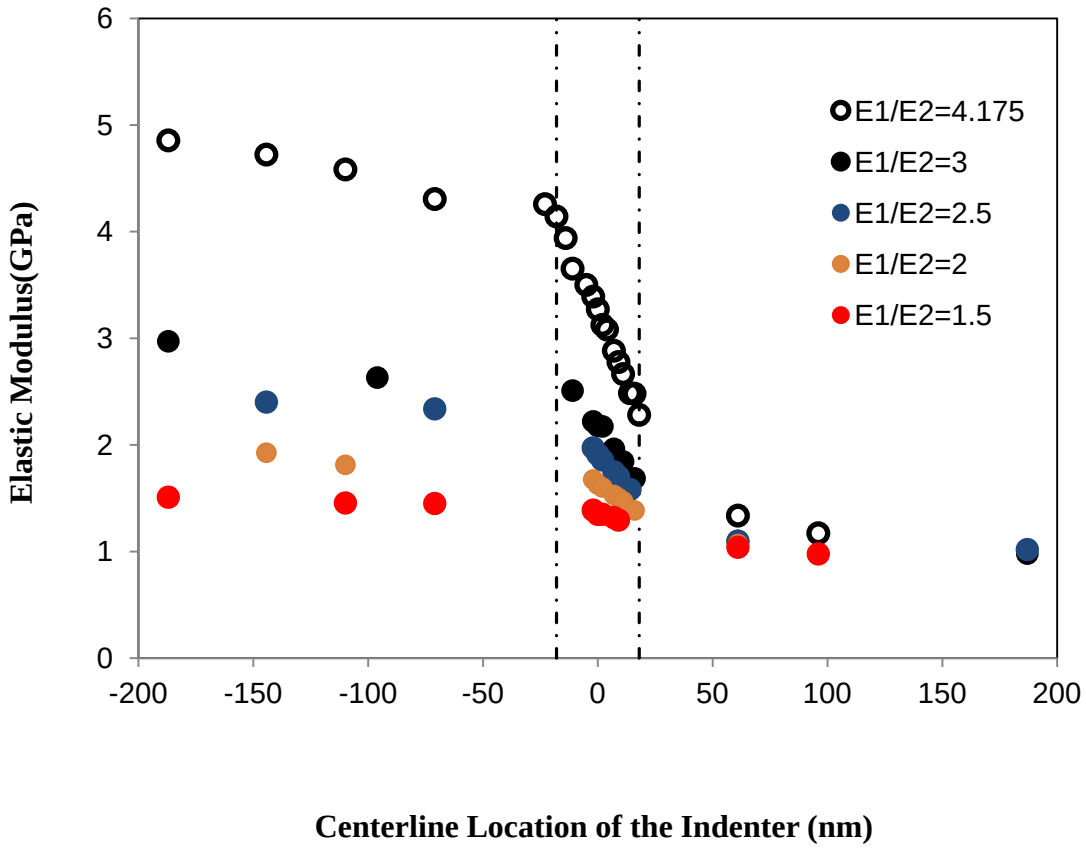

Figure 4.25 Modulus vs. position across the interface: R/T=1. Dashed lines indicate the boundaries of the interface.

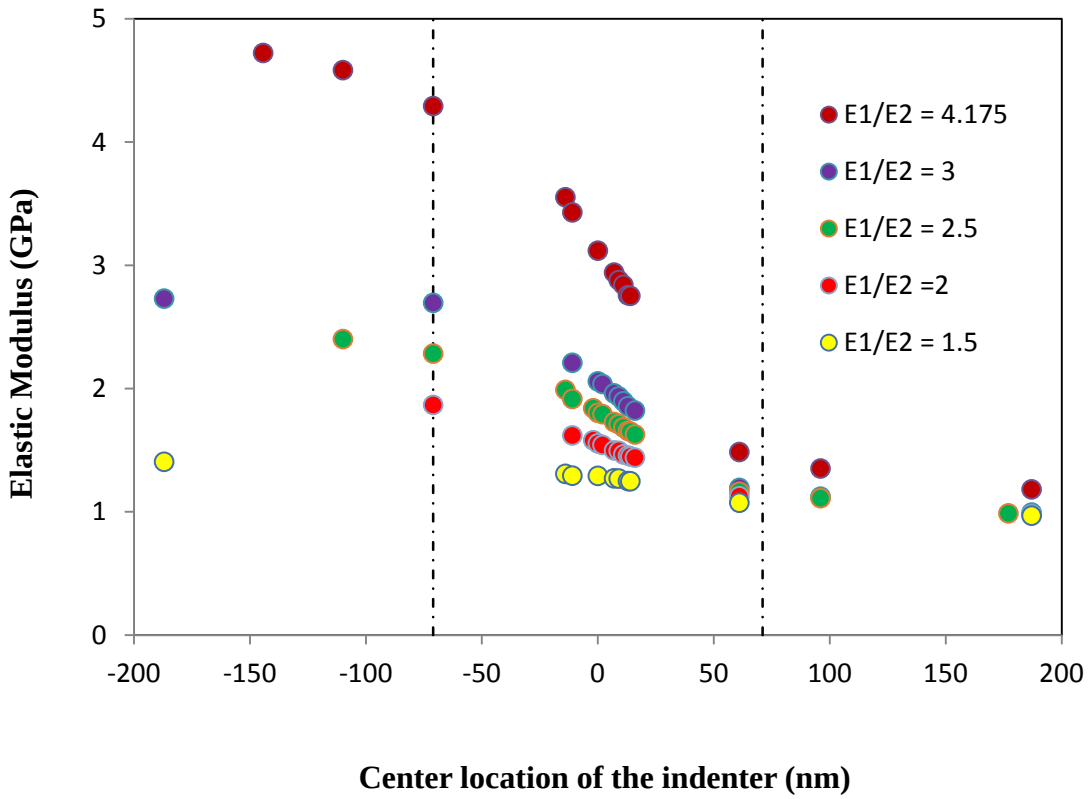

Figure 4.26 Modulus vs. position across the interface: R/T=2. Dashed lines indicate the boundaries of the interface.

Table 4.3. 3 Shows the comparison of modulus in the interface region for different ratios of elastic modulus of the oxidized to unoxidized regions and for different cases of R/T.

Elastic modulus in the interface (GPa)			
E_1/E_2	R/T=0	R/T=1	R/T=2
1.5	1.3402	1.349	1.2917
2	1.6158	1.628	1.5552
2.5	1.8852	1.9118	1.8032
3	2.6727	2.1792	2.0585
4.175	3.3057	3.2716	3.1186

From the table it can be seen that the values of elastic modulus in the interface region increases as the ratio of E_1/E_2 increased.

As shown in the von Mises contours (Figures 4.6-4.8), the interfaces exhibit inhomogeneous structure. Thus, the conventional analysis for calculating modulus from indentation experiments (Equations 4.5-4.10) becomes invalid. However, the results can still be used to show the variations of properties at the interfaces. Figures 4.24-4.26 show the variation of modulus across the interfaces for different radii of the indenter to the thickness ratios over a varying range of modulus ratios from 1.5 to 4.175. It can be seen that the modulus variations clearly shows the three regions in the materials: material1, the interface, and materials 2. Material 1 and material 2 are the regions that are far away from the interface and thus can be considered as homogeneous. The moduli of these two regions correspond to the values as obtained from testing homogeneous materials Figure

4.5. Within the transition regions (interfaces), the moduli decrease progressively. For all the structure analyzed, material 2 (the left region) has varying properties while material 1 (the right region) has the same properties. As we move from material 1 to material 2 of the sample we see that the modulus values for different E_1/E_2 ratios tend to be close to each other and reach a constant value.

Figures 4.21 - 4.23 shows the variation of hardness across the interfaces for different radii of the indenter to the thickness ratios over a varying range of modulus ratios from 1.5 to 4.175. The hardness results display the similar trends as the modulus, showing the variations of properties across the interfaces. However, in comparing to modulus values, which are calculated from formulas derived for homogeneous materials, the hardness values can be considered as "true" properties of the materials, since the hardness is simply defined as the average pressure within a contact area (H=P/A).

4.5 Effective Thickness of the Interface

One important objective of the present study is to estimate the effective interfacial thickness. A numerical method for estimating the interface thickness has been proposed recently by Yang et al [34], however, the analysis was based upon a 2-dimensional, wedge indentation model. Based on the hardness distribution across the interface, the apparent interfacial thickness (width), W, can be estimated [34]:

$$W = \frac{H_1 - H_2}{|k|} \qquad \text{---------- 4.11}$$

where H_1 and H_2 are the hardness of the two bulk materials, which are the hardness calculated from locations far away from the interface. The hardness data across the interface can be fit to a straight line and the slope is k.

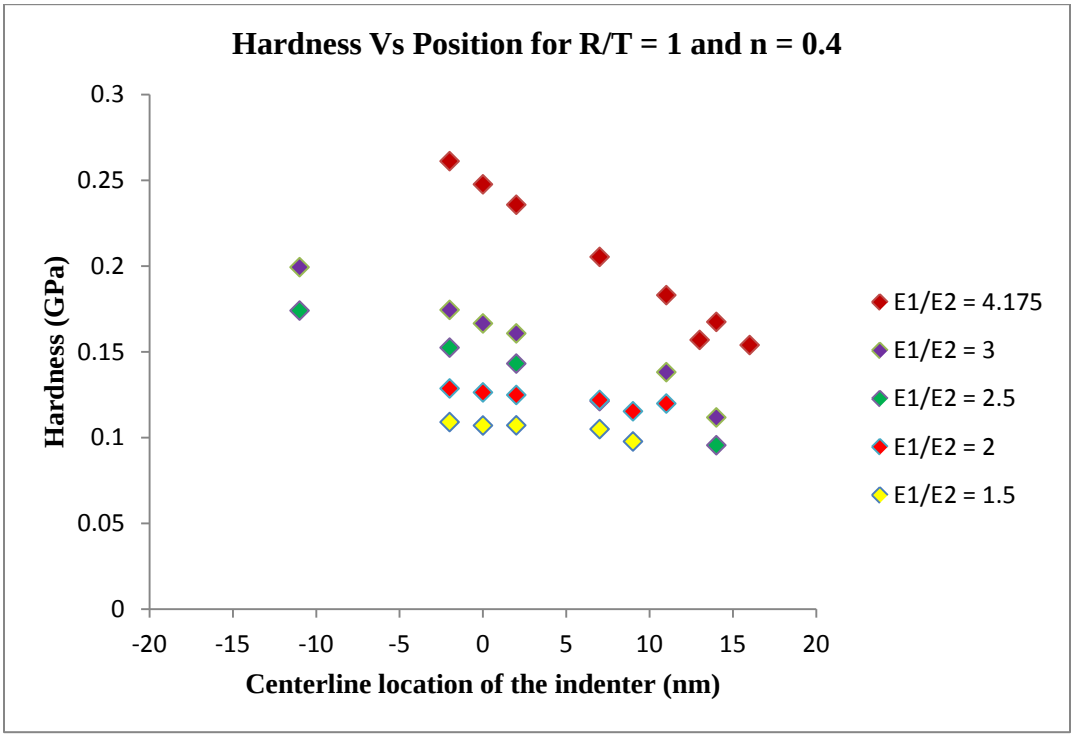

Figure 4.27 Shows the variation of hardness in the interface region for R/T = 1, n = 0.4 and for different modulus ratios of oxidized to unoxidized region varying from 4.175 to 1.5.

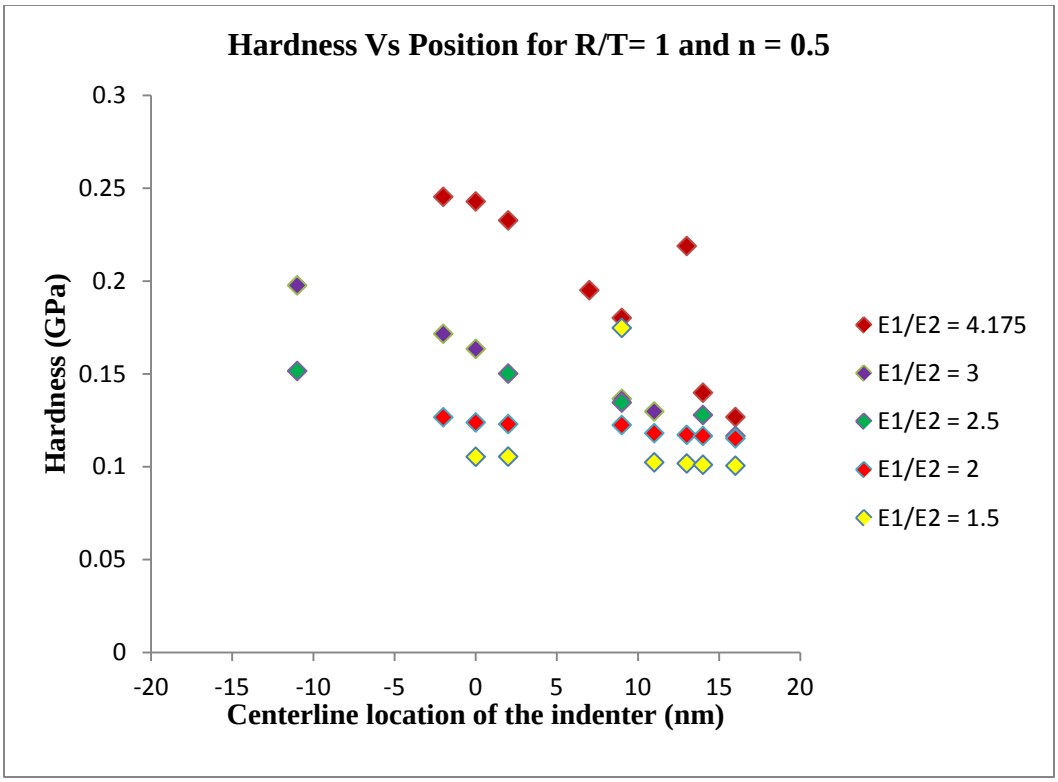

Figure 4.28 Shows the variation of hardness in the interface region for R/T = 1, n = 0.5 and for different modulus ratios of oxidized to unoxidized region varying from 4.175 to 1.5.

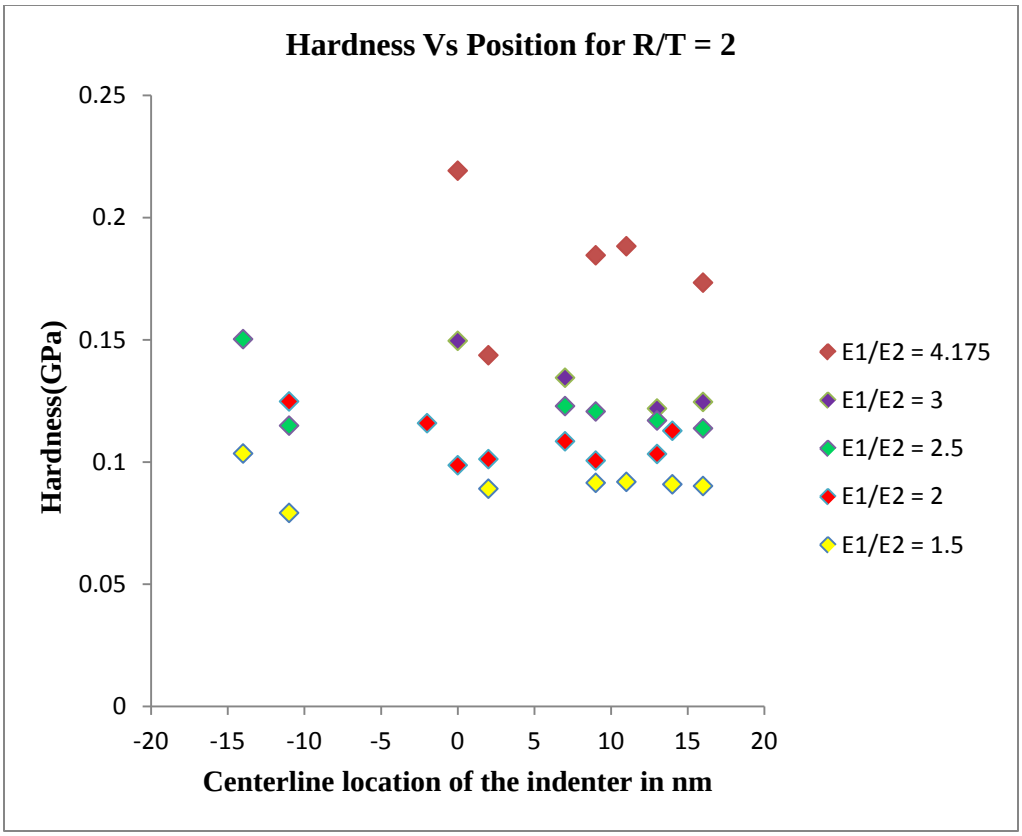

Figure 4.29 Shows the variation of hardness in the interface region for R/T = 2, n = 0.4 and for different modulus ratios of oxidized to unoxidized region varying from 4.175 to 1.5.

In all of the above Figures 4.27- 4.29 it can be seen that the hardness decreased across the interface from the oxidized to unoxidized zones. As the stiffness decreases it makes the interior of the sample more susceptible to fracture thus decreasing its resistance to fracture.

In the FE model, the true interfacial thickness (width), W_T, is known, so the relationship between apparent thickness (W) and true thickness (W_T) can be established, as seen in Figure 4.30. To make the results independent upon the indenter size, the thickness values are normalized with the indenter radius, R.

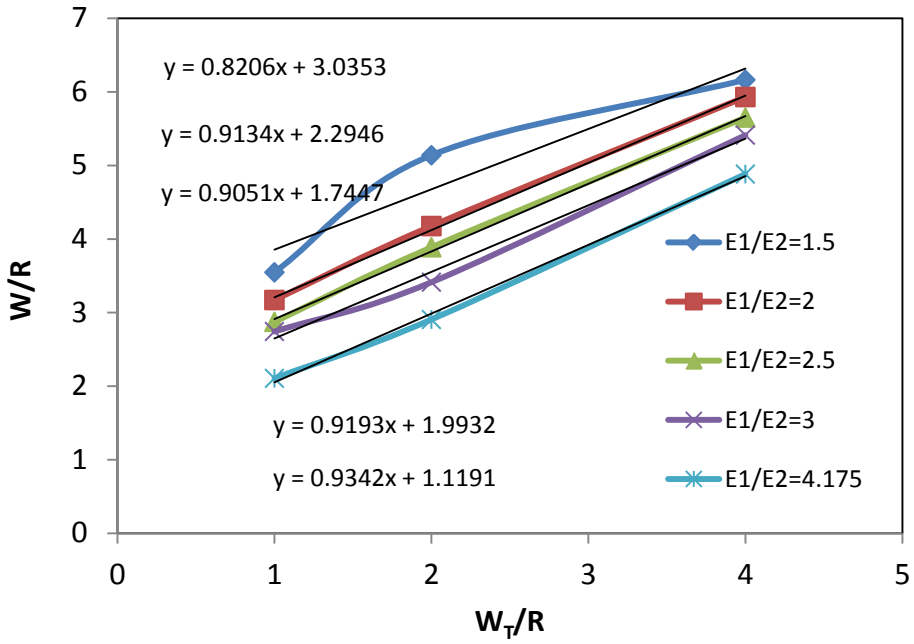

Figure 4.30 Plots of apparent interfacial thickness (W/R) and true interfacial thickness (W_T/R).

It is seen that the relationships between apparent thickness (W) and true thickness (W_T) follow the same trend, which can be simply expressed as [34]:

$$\frac{W}{R} = \zeta \frac{W_T}{R} + \frac{W_0}{R} \qquad \text{---------- 4.12}$$

Where ζ is the slope of each W-W_T curve corresponding to different material properties. The values of ζ are found to be identical with an average being: ζ=0.92. Although all curves have similar slopes, but they have different intercepts (W_0). Here W_0 can be interpreted as an uncertainty term, whose magnitude depends upon the material properties of the bimaterials, and can be expressed as:

$$\frac{W_0}{R} = f\left(\frac{E_1}{E_2}, \frac{\sigma_{y1}}{\sigma_{y2}}, \frac{n_1}{n_2}, \frac{\nu_1}{\nu_2}\right) \qquad \text{---------- 4.13}$$

where E, σ_y, n, ν are modulus, yield strength, strain hardening index, and Poisson's ratio, respectively, and the subscripts, 1 and 2, refer to two bulk materials next to the interface (Figure 3.10). Extensive analyses have been carried out on materials with a wide range of properties. A plot of W_0 vs. $\frac{E_1}{E_2}\frac{\sigma_{y1}}{\sigma_{y2}}\frac{n_1}{n_2} - 1$ is shown in Figure 4.31.

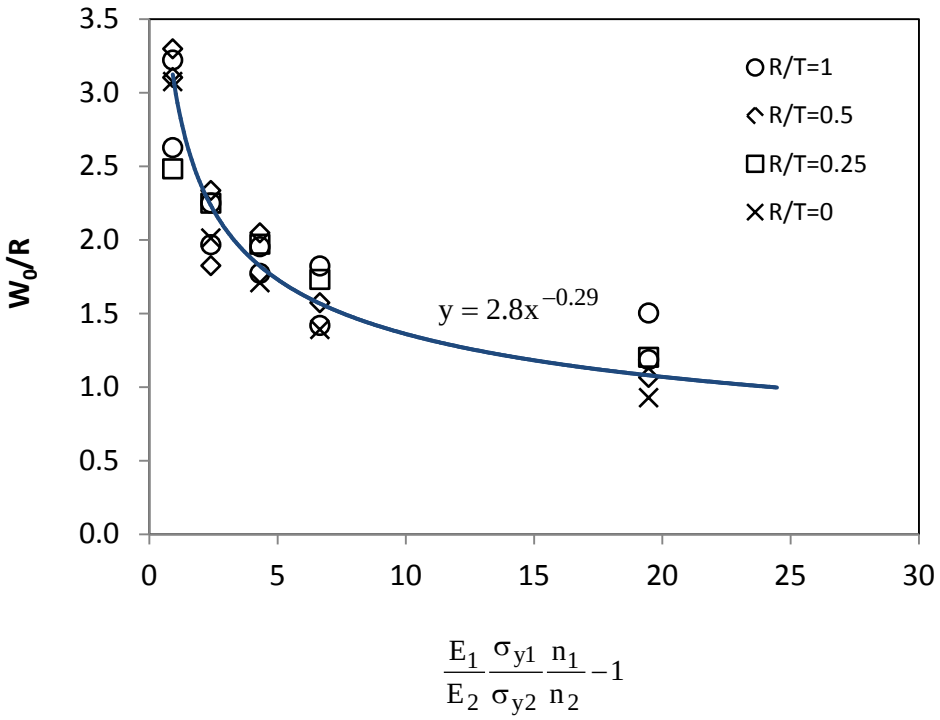

Figure 4.31 The generalized relations between interfacial thickness uncertainty (W_0/R) and material properties.

The data are seen to follow a power function [34]:

$$\frac{W_0}{R} = \beta\left(\frac{E_1}{E_2}\frac{\sigma_{y1}}{\sigma_{y2}}\frac{n_1}{n_2} - 1\right)^{-\alpha} \qquad \text{---------- 4.14}$$

where the two coefficients are estimated as: α=0.29 and β=2.8.

Combining Equations 4.12 and 4.14, the true interfacial thickness W_T for any unknown interface can then be estimated:

$$0.92\frac{W_T}{R} = \frac{W}{R} - 2.8\left(\frac{E_1}{E_2}\frac{\sigma_{y1}}{\sigma_{y2}}\frac{n_1}{n_2} - 1\right)^{-0.29} \quad \text{----------4.15}$$

CHAPTER 5 - CONCLUSIONS AND FUTURE WORK

High temperature polymers and polymer matrix composites have been increasingly used under extreme environments for applications across the automotive and aerospace industries. One major concern in using polymers and polymer matrix composites at such environments is the thermo-oxidative degradations of the polymer resins and the matrix-fiber interfaces. The interfaces (the regions between oxidized and unoxidized polymers, or between fiber and polymer matrix) are often the regions for failure initiations. Thus, the ability to characterize the physical and mechanical properties of the interfaces is paramount to the continued development and increased use of high temperature polymers in the industry.

The identifications of the interfaces in oxidized polymers or composites have been mostly achieved through various optical techniques, such as dark-field imaging, polarized light microscopy, and scanning electron microscopy. However, in many cases, the traditional optical methods fail to reveal the interfaces since the interfaces exhibit no visible differences from surrounding bulk materials. Furthermore, the traditional optical methods could not yield quantitative information about the properties of the interfaces. In this project, a navel technique, nanoindentation, has been used to identify the interfaces between dissimilar materials, and subsequently to evaluate the physical and mechanical properties across the interfaces. It is proposed to use a nanoindenter with spherical tip, <40 nanometers in radius, to indent across the interfaces of dissimilar materials. The nanoindentation tests have been conducted through 3-dimensional finite element simulations. Various interface models have been considered by varying the properties of the two dissimilar materials, including various combinations of modulus (E_1/E_2), yield strength (σ_{y1}/σ_{y2}), hardening index (n_1/n_2), interface sizes (R/T), etc.

The finite element simulations of indentation experiments were first conducted on homogeneous materials. For pure elastic materials, the indentation load-depth curves

were obtained and found to agree exactly with the Hertz analytical solution. For elastic-plastic materials, the load-depth curves were obtained, from which the modulus were calculated using standard Oliver-Pharr formula. The modulus results agreed well with the input values in the finite element models. All these indicate that the present finite element models (mesh, element sizes, boundary conditions, etc.) are valid for simulating the indentation of a half-space by a rigid sphere.

The finite element simulations of indentation experiments were then conducted on dissimilar materials containing interfaces. A large number of interface scenarios were investigated, including various combinations of modulus (E_1/E_2), yield strength (σ_{y1}/σ_{y2}), hardening index (n_1/n_2), interface sizes (R/T), Poisson ratio (ν), etc. Results show that the stress distributions at the interfaces are strongly affected by the properties of the surrounding materials. By indenting across the interfaces, the mechanical properties (stiffness, modulus, and hardness) were calculated. The mechanical properties at interfaces are seen to increases with the increase of modulus ratios E_1/E_2, yield strength ratios σ_{y1}/σ_{y2}, and hardening index ratios n_1/n_2, and with the decrease of interface size (R/T).

Finally, a quantitative equation for predicting the sizes (thickness) of the interfaces by nanoindentation has been established. Nanoindentation has been extensively used to examine the mechanical properties of low-dimensional materials structures, but it has not been frequently used to evaluate the sizes of the interfaces. Moreover, an accurate formula for quantifying the interface size (thickness) is lacking. Considering the hardness as the true properties of the interfaces, the apparent interfacial thickness (W) could be estimated. Then, the apparent interfacial thickness was found to relate to the true interfacial thickness (W_T) through a simple power-law function.

Future Works:

The nanoindentation method has been proposed to identify the interfaces between dissimilar materials, and subsequently to evaluate the physical and mechanical properties across the interfaces. The method has been validated by conducting a large number of virtual experiments through 3-dimensional finite element simulations, by varying the properties of the two dissimilar materials, including various combinations of modulus (E_1/E_2), yield strength (σ_{y1}/σ_{y2}), hardening index (n_1/n_2), interface sizes (R/T), Poisson's ratio (ν), etc. Quantitative model for predicting the interface sizes has been established.

Future work may include conducting physical experiments to test and refine the model. The materials properties (E_1/E_2, σ_{y1}/σ_{y2}, n_1/n_2, R/T, ν) used in the present simulations were based on the properties of typical high temperature polymers and composites such as PMR-15 resin and carbon fiber reinforced PMR-15 composites. Specimens from such materials have been previously obtained. It is thus suggested to conduct nanoindentation experiments on those materials and then to refine the model. One challenge that may occur in actual experiments would be to obtain sufficient data points across an interface, due to its small size. A typical thickness (width) of an interface in oxidized polymer or fiber reinforced composite may be just a few microns or less. That essentially limits the number of nanoindentation tests that can be performed (especially considering the effect of stress field from neighboring indents).

REFERENCES

1. G. A. Schoeppner, G. P. Tandon, and K. V. Pochiraju, *"Predicting Thermo-Oxidative Degradation and Performance of High Temperature Polymer Matrix Composites," in Multiscale Modeling and Simulation of Composite Materials and Structures*, s.l: Springer, pp 359-462, 2007.
2. G. A. Schoeppner and D. B. Curliss, *"Model-based design for composite materials life management," in 9th AIAA/ISSMO Symposium on Multidisciplinary Analysis and Optimization*, Atlanta,GA , 2002.
3. G. P. Tandon, K. V. Pochiraju, and G. A. Schoeppner, "Modeling of oxidative development in PMR-15 resin," *Polymer Degradation and Stability*, vol. 91, no. 8, pp. 1861-1869, 2006.
4. E. R. Ripberger and G. P. Tandon, G. A. Schoeppner, "Experimental Techniques for Characterizing Thermo-Oxidative Behavior in High-Temperature Polyimide Composites", Proceeding of SEM Annual Conference & Exposition on Experimental and Applied Mechanics, 2005.
5. Wang, Y. and Hahn, T.H., "AFM characterization of the interfacial properties of carbon fiber reinforced polymer Composites subjected to hygrothermal treatments", Composites Science and Technology 67 (2007) 92–101.
6. Lu, Y.C., G. P. Tandon, D.C., Jones, G. A. Schoeppner, *"Elastic and viscoelastic characterization of thermally-oxidized polymer resin using nanoindentation"*, Journal of Mechanics of Time-Dependent Materials, 13: 245–260 (2009).
7. J. L. Broeckert, "Effects of Prior Aging at Elevated Temperature in Air and in Argon Environments on Creep Response of PMR-15 Neat Resin at 288°C," Master's Thesis, WPAFB OH, 2007.
8. Seung-Hwag Lee, Siqun Wang, George M.Pharr, Haitao Xu, "Evaluation of interphase properties in a cellulose fiber-reinforced polypropylene composite by nanoindentation and finite element analysis", www.sciencedirect.com, Composites: Part A 38(2007) 1517-1524.

9. T.D.Downing, R.Kumar, W.M.Cross, L.Kjerengtroen and J.J.Kellar, "Determining the interphase thickness and properties in polymer matrix composites using phase imaging atomic force microscopy and nanoindentation", J.Adhesion Sci.Technol., Vol. 14, No. 14, pp. 1801-1812(2000).
10. Bhattacharya, A.K. and Nix, W.D.,"*Finite Element Simulation of Indentation Experiments, International Journal of Solids and Structures",*Vol. 24, pp. 881-891, 1988.
11. Bhattacharya, A.K. and Nix, W.D.,"*Finite Element Analysis of Cone Indentation, International Journal of Solids and Structures",* Vol. 27, pp. 1047-1058, 1990.
12. Bolshakov, A. and Pharr, G.M.,"*Influences of Pileup on The Measurement of Mechanical Properties by Load and Depth Sensing Indentation Techniques"*,s.l, J Mater Res, pp. 13p1049, 1998.
13. Larsson,L.,Giannkopoulos,A.E.,Soderlund,E., Rowcliffe, D.J. and Vestergaard, R., *"Analysis of Berkovich Indentation",* s.l. : International Journal of Solids and Structures, Vols. Volume 33, 221, 1996.
14. Shih, C.W., Yang, M. and Li, J.C.M.,"*Effect of Tip Radius on Nano-indentation",* s.l. : J. Mater. Res. 6, pp. 2623-2628, 1991.
15. Cheng, Y.T. and Cheng, C.M.,"*Further Analysis of Indentation Loading Curves: Effects of Tip Imperfection on Mechanical Property Measurements",* s.l. : Journal of Materials Research, pp. 13, 1059, 1998.
16. Shu, J.Y. and Fleck, N.A.,"*The Prediction of a Size Effect in Micro-Indentation",* s.l. : Int. J. Solids Struct. 35, pp. 1363-1383, 1998.
17. Mesarovic, S.D. and Fleck, N.A., *"Spherical Indentation of Elastic-Plastic Solids",* s.l. : Proceedings of Royal Society of London, pp. 455,2707-2728, 1999.
18. Taljat, B., Zacharia, T. and Kosel, *"New Analytical Procedure To Determine Stress-Strain Curve from Spherical Indentation Data",* F. s.l. : INT. J. Solids Struct. 35, pp. 4411-4426, 1998.
19. Taljat, B. and Pharr, G.M., *"Developments of Pile-Up During Spherical Indentation of Elastic-Plastic Solids",* s.l. : International Journal of Solids and Structures, Vol. 41,pp. 3891-3904, 2004.

20. King, R.B.,*"Elastic Analysis of Some Punch Problems For a Layered Medium"*, s.l. : Int J Solids Struct, p. 23p1657, 1987.

21. Doerner, M.F., Gardner, D.S and Nix, W.D., *"Plastic Properties of Thin Films on Substrates as Measured by Submicron Indentation Hardness and Substrate Curvature Techniques"*, Res. 1 (6), s.l. : J. Mater., Nov/Dec, 1986.

22. Djabella, H. and Arnell, R.D., *"Finite Element Analysis of The Contact Stresses In An Elastic Coating on and Elastic Substrate"*, *Thin solid films*, pp. 213, 205-219, 1992

23. Xun, Cai,*"Effect of Friction in Indentation Hardness Testing: a Finite Element Study"*, 12, s.l. : Journal of material science letters., 1993.

24. Page, T.F. and Hainsworth, S.V.,*"Using Nanoindentation Techniques For The Characterization of Coated Systems: A Critique"*, s.l. : Surf Coat Technol; p. 61p201, 1993.

25. Mesarovic, S.D. and Fleck, N.A., *"Spherical Indentation of Elastic-Plastic Solids"*, s.l. : Proceedings of Royal Society of London, pp. 455,2707-2728, 1999.

26. *Hibbit, Karlson and Sorenson Inc, Pawtucket, RI. ABAQUS, 2007, ABAQUS Users' Manual,. [online]* http://web.mit.edu/calculix_v2.0/CalculiX/ccx_2.0/doc/ccx/node15.html.

27. Hertz, H. s.l. : J. Reine. Angew. Math., *"On the Contact of Elastic Solids"*, pp. 92 156-171, 1882.

28. MTS Systems Corporation. *XP User's Manual: TestWorks® 4 Software for Nanoindentation Systems, Ver.#16.* 2002. D1418XPA-10629.

29. Oliver, W. C. and Pharr, G. M., " *An improved technique for determining hardness and elastic modulus using load and displacement sensing indentation experiments."*, Journal of Materials Research, Vol. 7, pp. 1564-1583, 6/1992.

30. Oliver, W. C. and Pharr, G. M., *"Measurement of hardness and elastic modulus by instrumented indentation: Advances in understanding and refinements to methodology."*, Journal of Materials Research, Vol. 19, pp. 3-20, 1/ 2004.

31. Metcalfe, A.G., *"Interface in metal matrix composites"*, Composite Materials, Vol 1., New York, Academic Press, 1974.

32. Kim, J.K. and Mai, Y.W., *"Interfaces in Composites"*, In: Chou. T.W., Editor, Materials Science and Technology: structure and properties of composites, 13, Weinheim, Germany: VCH 1993, p. 229-289.
33. Lu, Y.C. and Shinozaki, D.M., *"Effects of substrate constraint on micro-indentation testing of polymer coatings"*, Materials Science and Engineering A 396 (2005) 77–86.
34. Yang, C., Lo, C-T., Bastawros, A.F. and Narasimhan, B., *"Measurements of diffusion thickness at polymer interfaces by nanoindentation: A numerically calibrated experimental approach"*, J. Mater. Res., Vol. 24, No. 3, (2009).

VITA
Sesha Spandana Pulla

Born December 17th, 1986 in Visakhapatnam, India

Education

MS, Mechanical Engineering, University of Kentucky (UK), Lexington, KY (September, 2011)

BE, Mechanical Production and Industrial Engineering, GITAM University, Andhra Pradesh, India (April, 2008)

Professional Experience

- Graduate Research Assistant – 08/2009 – 05/2011

  University of Kentucky – College of Engineering, Lexington, KY
- Graduate Teaching Assistant – 08/2009 – 12/2009

  University of Kentucky – College of Engineering, Lexington, KY
- Industrial trainee – 05/2007 – 06/2007

  Hindustan Shipyard Limited – Visakhapatnam, Andhra Pradesh, India

Papers & Presentations

- Sesha Spandana Pulla, "Contact stress analysis on a gear tooth", Presented at SAE Collegiate club, SRM University, India, 02/2007.
- Sesha Spandana Pulla, "Stress analysis on a gear tooth using FEM models", Presented at SAMVID '07, MVGR, COE, India, 03/2007.
- Sesha Spandana Pulla, "Optimization of Blast furnace burden system", Presented at MESCON '07,Andhra University,India,09/2007
- Sesha Spandana Pulla, "Bending stress analysis on a gear tooth", Presented at Institute of Engineers (India), COE, GITAM University, India, in the academic year 2007-2008.
- Sesha Spandana Pulla, "Tool Wear Monitoring with Indirect Methods" Presented at IEI Student Civil Chapter – Institute of Engineers (INDIA) Student Chapter (CIVIL), organized by Civil Engineering Department of GITAM University, College of Engineering, India.
- David C. Jones, S. Spandana Pulla, Y. Charles Lu **"**Mechanical Properties of Polymer Composites Used in Oxidizing Environments: A Review**",** Presented at Society of Automotive Engineering (SAE) 2010 Congress, Indianapolis, 06/2010 was accepted as a journal at SAE International Journal of Materials and Manufacturing, 3(1): 73-70 (2010).

- Spandana Pulla, Johnson Joseph, Jared Fulcher, Y Charles Lu, Fuqian Yang, Haluk Karaca, “High Temperature Polymer Matrix Composites for Aerospace and Space Applications”, Poster presented at 15th KY EPSCoR conference,Lexington,KY,05/2010.